

---


Electronic Theses and Dissertations, 2004-2019

---

2010

## Characterization And Modeling Of A High Power Thin Disk Laster

Omar Rodriguez-Valls  
*University of Central Florida*

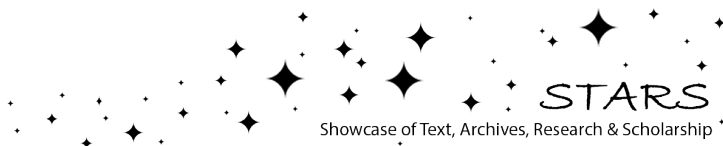
 Part of the [Electrical and Electronics Commons](#)  
Find similar works at: <https://stars.library.ucf.edu/etd>  
University of Central Florida Libraries <http://library.ucf.edu>

This Masters Thesis (Open Access) is brought to you for free and open access by STARS. It has been accepted for inclusion in Electronic Theses and Dissertations, 2004-2019 by an authorized administrator of STARS. For more information, please contact [STARS@ucf.edu](mailto:STARS@ucf.edu).

---

### STARS Citation

Rodriguez-Valls, Omar, "Characterization And Modeling Of A High Power Thin Disk Laster" (2010).  
*Electronic Theses and Dissertations, 2004-2019*. 4351.  
<https://stars.library.ucf.edu/etd/4351>



CHARACTERIZATION AND MODELING OF A HIGH POWER THIN DISK  
LASER

by

OMAR R. RODRIGUEZ  
B.S. University of Central Florida, 2008

A thesis submitted in partial fulfillment of the requirements  
for the degree of Master of Science  
in the School of Electrical Engineering and Computer Science  
in the College of Engineering and Computer Science  
at the University of Central Florida  
Orlando, Florida

Summer Term  
2010

Major Professor: Martin C. Richardson

## ABSTRACT

High power lasers have been adapted to material processing, energy, military and medical applications. In the Laser Plasma Laboratory at CREOL, UCF, high power lasers are used to produce highly ionized plasmas to generate EUV emission. This thesis examines the quality of a recently acquired high power thin disk laser through thermal modeling and beam parameter measurements.

High power lasers suffer from thermally induced issues which degrade their operation. Thin disk lasers use an innovative heat extraction mechanism that eliminates the transverse thermal gradient within the gain medium associated with thermal lensing. A thorough review of current thin disk laser technology is described.

Several measurement techniques were performed on a high power thin disk laser. The system efficiencies, spectrum, and temporal characteristics were examined. The laser was characterized in the far-field regime to determine the beam quality and intensity of the laser.

Laser cavity simulations of the thin disk laser were performed using LASCAD. The induced thermal and stress effects are demonstrated. Simulated output power and efficiency is compared to those that have been quantified experimentally.

*To my family.*

## ACKNOWLEDGMENTS

The culmination of this thesis represents a step in my life which I could not have accomplished without the help of many people. I foremost thank my advisor, Dr. Martin Richardson, for all of the many opportunities he has provided and his invaluable guidance and advice. I also wish to thank my committee members Dr. Aravinda Kar and Dr. Peter Delfyett for their valuable time in reading this thesis. I thank Dr. Lawrence Shah for his advice and many intuitive and constructive conversations.

I give my honest gratitude to my peers in the EUV group: Reuvani Kamtaprasad, John Szilagyi, and Nathan Bodnar for valuable ideas that helped me finish my thesis. Many thanks to Somsak (Tony) Teerawattanasook for his help on many occasions. I am also grateful to the rest of my colleagues from the Laser Plasma Laboratory at UCF for advice, equipment, and contributions to my work.

I would like to express my gratitude towards several employees at TRUMPF GmbH +Co. KG, including Christian Stolzenburg, Wolfgang Schuele, and Dr. Sascha Weiller from Trumpf Laser GmbH and Thomas Ossek from Trumpf Inc. The provided training and assistance with several matters regarding the laser system was a major contribution to this work.

I would also like to thank to Matthias Wohlmuth (University of Erlangen-Nuremberg) and Dr. Konrad Altmann (LAS-CAD GmbH) for their invaluable assistance and contributions to my work consisting LASCAD simulations.

My final recognition goes to my family. Thank you for your motivation, inspiration and for believing in me.

## TABLE OF CONTENTS

<b>LIST OF FIGURES</b> . . . . .	<b>x</b>
<b>LIST OF TABLES</b> . . . . .	<b>xii</b>
<b>LIST OF ACRONYMS</b> . . . . .	<b>xiii</b>
<b>CHAPTER 1 : INTRODUCTION</b> . . . . .	<b>1</b>
<b>CHAPTER 2 : THE THIN DISK LASER</b> . . . . .	<b>5</b>
2.1 Solid State Lasers . . . . .	5
2.1.1 Pumping Schemes . . . . .	5
2.1.2 Laser Resonator . . . . .	7
2.1.3 Pulse Generation . . . . .	9
2.1.4 Architecture . . . . .	11
2.2 Gain Media . . . . .	15
2.2.1 Gain Requirements . . . . .	15
2.2.2 Yb:YAG . . . . .	16

2.3	Technology . . . . .	24
2.3.1	Thermal Management . . . . .	24
2.3.2	Pumping . . . . .	26
2.3.3	Laser Resonator . . . . .	29
<b>CHAPTER 3 : TRUMPF TRUMICRO 7050 SETUP . . . . .</b>		<b>30</b>
3.1	Cavity Design . . . . .	30
3.2	Pumping Scheme . . . . .	30
3.3	Thin Disk Design . . . . .	31
3.3.1	Disk Enclosure . . . . .	34
3.3.2	Cooling Finger . . . . .	34
3.4	Pulse Generation . . . . .	36
3.4.1	Cavity Dumping . . . . .	36
3.5	System Design . . . . .	40
3.5.1	Electrical System . . . . .	40
3.5.2	Control System . . . . .	40
3.5.3	Thermal Managment . . . . .	41
3.5.4	Humidity Control System . . . . .	41
<b>CHAPTER 4 : LASER CHARACTERIZATION . . . . .</b>		<b>43</b>



4.1	Continuous Wave Operation . . . . .	43
4.1.1	Intracavity Power . . . . .	44
4.1.2	Polarizer Output Coupling . . . . .	45
4.2	Pulsed Operation . . . . .	46
4.2.1	Energy Output . . . . .	46
4.2.2	Average Power . . . . .	47
4.2.3	Pulse Duration . . . . .	48
4.2.4	Peak Power . . . . .	50
4.3	Beam Quality . . . . .	50
4.3.1	Measurement Technique . . . . .	52
4.4	Spectral Characterization . . . . .	54
4.5	Laser Intensity . . . . .	55
4.5.1	Brightness . . . . .	55
4.5.2	Intensity . . . . .	57
4.6	Improvements . . . . .	58
4.6.1	Damage Thresholds . . . . .	58
<b>CHAPTER 5 : LASER MODELING . . . . .</b>		<b>59</b>
5.1	LASCAD . . . . .	59

5.1.1	Finite Element Analysis . . . . .	60
5.1.2	Laser Power CW . . . . .	61
5.1.3	Beam Propagation . . . . .	62
5.1.4	Dynamic Multimode Analysis . . . . .	63
5.2	Design . . . . .	63
5.2.1	Cavity Layout . . . . .	63
5.2.2	Pumping Technique . . . . .	64
5.3	Results . . . . .	65
5.3.1	Finite Element Analysis . . . . .	65
5.3.2	Laser Power CW . . . . .	68
<b>CHAPTER 6 : CONCLUSION . . . . .</b>		<b>69</b>
6.1	Future Work . . . . .	70
<b>APPENDIX A : Copyright Permission Letter . . . . .</b>		<b>71</b>
<b>LIST OF REFERENCES . . . . .</b>		<b>73</b>

## LIST OF FIGURES

Figure 2.1	Laser Resonator Stability Criterion Plot . . . . .	8
Figure 2.2	Energy Levels . . . . .	17
Figure 2.3	Yb:YAG Energy Levels . . . . .	18
Figure 2.4	Yb:YAG Cross Section Spectra . . . . .	19
Figure 2.5	Thin Disk Cooling Configuration . . . . .	25
Figure 2.6	Thin Disk Multiple Pass Pumping . . . . .	27
Figure 3.1	Trumpf TruMicro 7050 Cavity Layout . . . . .	31
Figure 3.2	Trumpf TruMicro 7050 Laser Cavity . . . . .	32
Figure 3.3	Trumpf TruMicro 7050 Pump Laser Diodes . . . . .	33
Figure 3.4	Trumpf TruMicro 7050 Disk Fluorescence . . . . .	34
Figure 3.5	Trumpf TruMicro 7050 Pump Laser Diodes . . . . .	35
Figure 3.6	Trumpf TruMicro 7050 Cavity Dumping Timing Diagram . . . . .	37
Figure 3.7	Trumpf TruMicro 7050 Pockels Cell . . . . .	38
Figure 4.1	Trumpf TruMicro 7050 CW Efficiencies . . . . .	44

Figure 4.2	Trumpf TruMicro 7050 Energy Output . . . . .	47
Figure 4.3	Trumpf TruMicro 7050 Pulsed Efficiencies . . . . .	48
Figure 4.4	Trumpf TruMicro 7050 Pulse Duration at Various Frequencies . . . . .	49
Figure 4.5	Trumpf TruMicro 7050 Pulse . . . . .	50
Figure 4.6	Trumpf TruMicro 7050 Peak Powers . . . . .	51
Figure 4.7	Trumpf TruMicro 7050 Beam Measurement Technique . . . . .	53
Figure 4.8	Trumpf TruMicro 7050 Far-Field Beam Profiles at 20% Pump Power . . . . .	55
Figure 4.9	Trumpf TruMicro 7050 Far-Field Beam Profiles at 50% Pump Power . . . . .	56
Figure 5.1	LASCAD Cavity Configuration . . . . .	64
Figure 5.2	Thin Disk Thermal Visualizations . . . . .	66
Figure 5.3	Thin Disk Structural Effects Visualizations . . . . .	67
Figure 5.4	Measured vs Simulated Efficiencies . . . . .	68

## LIST OF TABLES

Table 2.1 Comparison of Different Thin Disk Laser Gain Media's Characteristics at Room Temperature . . . . .	23
---	----

## LIST OF ACRONYMS

AOM	—	Acousto-Optic Modulator
AR	—	Anti Reflective
ASE	—	Amplified Spontaneous Emission
BBO	—	Beta Barium Borate
CW	—	Continuous Wave
DI	—	Deionized
EM	—	Electromagnetic
EOM	—	Electro-Optic Modulator
EUV	—	Extreme Ultraviolet
FWHM	—	Full Width at Half Maximum
HEPA	—	High Efficiency Particulate Absorbing
HeNe	—	Helium-Neon Laser
HR	—	Highly Reflective
HVM	—	High Volume Manufacturing
LASCAD	—	Laser Cavity Analysis & Design
LASER	—	Light Amplification by Stimulated Emission of Radiation
MASER	—	Microwave Amplification by Stimulated Emission of Radiation
ND	—	Neutral Density
Nd:YAG	—	Neodymium Doped Yttrium Aluminum Garnet
Nd:YVO <sub>4</sub>	—	Neodymium Doped Yttrium Vanadate
OC	—	Output Coupler
PC	—	Pockel's Cell
QD	—	Quantum Defect
QE	—	Quantum Efficiency
QWP	—	Quarter Wave Plate
SA	—	Saturable Absorber
TEM	—	Transverse Electromagnetic
TFP	—	Thin Film Polarizer
Tm:YAG	—	Thulium Doped Yttrium Aluminum Garnet
Yb:KYW	—	Ytterbium Doped Potassium Yttrium Tungstate
Yb:YAG	—	Ytterbium Doped Yttrium Aluminum Garnet

# CHAPTER 1

## INTRODUCTION

In the year 1955, the first instance of stimulated emission was demonstrated by Charles H. Townes [1]. Townes effectively used ammonia ( $\text{NH}_3$ ) to amplify microwaves. The device was called the MASER, an acronym for microwave amplification by stimulated emission of radiation. After such demonstration, it was speculated that producing an optical maser would be possible. In 1958, Schawlow and Townes published a thorough theory behind optical masers [2]. It was not until May of 1960 that the first optical maser was demonstrated by Miaman [3]. The term LASER, an acronym for light amplification by stimulated emission of radiation, was established as the official name for such devices. At the time, there were no practical applications for this new laser technology.

Afterwards, different kinds of laser technologies emerged with different wavelengths and powers. Throughout the years, scientists and engineers have adapted the use of lasers to manufacturing processes in order to increase the efficiency and performance of the end products. The industrial laser materials processing industry, which yields over \$1B of revenue every year, is one of the main consumers and contributors to laser technology [4]. For industry, lasers are used for cutting, welding, and processing [5]. Lasers have also begun to be used for medicinal purposes. Some of the most common medical fields using lasers include

ophthalmology [6], dentistry [7], and dermatology [8]. The biomedical laser field has emerged by promising to simplify procedures and enhance the patient's life and healing time. All of the aforementioned applications require lasers of different wavelengths and power.

A market that incorporates laser technologies is the chip lithography industry. The semiconductor industry, which engrosses almost \$200B annually, is continually exploring ways to produce better chips [9]. The future lies on EUV technologies, which would use 13.5 nm light to produce chips with features which are nearly half the size of today's most advanced chips. It is estimated that by 2014, EUV will be the predominate chip manufacturing standard [10, 11].

The extreme ultraviolet (EUV) group in the Laser Plasma Laboratory in CREOL, UCF is dedicated to producing high powered EUV sources for lithography. To obtain EUV radiation, a tin compound is irradiated with a high power laser. This produces highly ionized plasma, which generates EUV and other wavelengths. Due to the atmospheric absorption of EUV wavelengths, the droplets are enclosed in a vacuum chamber. The EUV light from this plasma is then collected by means of special multi-layered mirrors. These multi-layered mirrors are made up of alternating thin film levels of high and low atomic number ( $Z$ ) elements. The mirrors used by the EUV team, which are composed of levels of Molybdenum (high  $Z$ ) and Silicon (low  $Z$ ), have a maximum reflectivity of approximately 67.5% at 13.5nm [12]. The debris that is expelled from the target due to the irradiation from a laser travels through the chamber. If debris lands in the optics, their lifetime and reflectivity are reduced. The EUV community experimented with solid tin, but this generated a great amount of debris.



In order to extend the optics' lifetime, the EUV group at UCF developed a mass-limited droplet system. 30  $\mu\text{m}$  diameter water droplets, doped with  $10^{15}$  tin atoms are generated within the vacuum chamber at a defined frequency. If an intense laser pulse covers the entire droplet, the droplet can be fully ionized, causing maximum EUV emission with minimal debris [13, 14, 15].

The EUV community has established several requirements for high volume manufacturing (HVM). For maximum EUV generation from a laser produced plasma, the required laser intensity is in the order of  $1 \times 10^{11} \text{W/cm}^2$  [12]. HVM requires 115 W of EUV power at intermediate focus [13]. Measurements of laser produced EUV sources have demonstrated that near-IR lasers, most notably  $1\mu\text{m}$  sources, yield a higher conversion efficiency (CE) than lasers with other wavelengths, such as excimer and  $\text{CO}_2$  lasers [13]. To satisfy these requirements, the EUV team at UCF has used time-multiplexed high power diode pumped solid-state lasers. These lasers produced approximately 1.2 kW of power each with a wavelength of  $1.064\mu\text{m}$ . However, these rod based laser systems suffer greatly from thermal problems, which affect the beam profile quality.

Thin disk lasers have emerged as a new and very efficient laser technology. This type of laser uses a very thin laser gain media, which is typically less than 1 mm in thickness. Many of the thermal effects that limit rod lasers can be significantly reduced due to improved heat extraction. Because of this, thin disk lasers yield a better beam quality than conventional rod based laser systems. Yb:YAG predominates as the gain medium used for most thin disk lasers due to the thermal and gain characteristics of this medium [16].

The EUV group has recently acquired a high powered thin disk laser. This system, the TruMicro 7050 made by TRUMPF Laser GmbH, is efficient and reliable. Initial characterization and set up was performed in Schramberg, Germany at TRUMPF Laser GmbH. The final characterization and modeling was performed at CREOL, UCF. This is the first laser of its kind in the US. The TruMicro 7050 is capable of reaching continuous wave (CW) powers beyond 1 kW or can produce 80 mJ pulses with 30 ns duration.

A thin disk lasers model was generated by using LASCAD, a laser cavity analysis and design software made by LAS-CAD GmbH. LASCAD allows the user to simulate a laser cavity to model laser power, energy, pulse duration, beam quality, thermal effects, material stresses, and other factors for lasers operating in CW and pulsed lasers. At the moment, LASCAD is not capable to simulate a laser system as complex as the Trumpf TruMicro 7050 due to several constraints. LASCAD only allows for 3 and 4-level systems and the temporal laser behavior algorithms only works for 4-level systems. For this thesis, the model was used to demonstrate the Trumpf cavity in the CW regime. This is critical to understanding the constraints limiting laser performance. For EUV generation, it is necessary to produce  $1 \times 10^{11} \text{W/cm}^2$  on target. Furthermore, a long focal length greatly simplifies the EUV generation and collection setup. Thus, the laser must provide the highest pulse energy with the highest possible beam quality.

## CHAPTER 2

### THE THIN DISK LASER

This chapter is dedicated to thin disk laser technology. First, a thorough explanation of laser fundamentals is presented, with a focus on solid state lasers. This is followed by a description of thin disk gain media requirements. The last section discusses current thin disk laser technology in detail.

#### 2.1 Solid State Lasers

##### 2.1.1 Pumping Schemes

Laser operation is established by stimulating a material causing the atoms within to emit electromagnetic radiation. Typically, this stimulation is achieved by electrical (ie. gas lasers) or optical pumping (ie. solid-state lasers). When the material is pumped, the atoms reach an excited state energy level. Once energized, these particles will spontaneously decay into a lower energy state. During this decay process, electromagnetic radiation and/or heat are emitted. If an optical cavity is built around the gain medium, it is possible to stimulate the transition from the upper to lower energy level and form a laser.

When the first laser was introduced by Maiman in 1960, a flashlamp was used to pump the ruby ( $\text{Cr}^{3+}:\text{Al}_2\text{O}_3$ ) medium. The ruby contained silver coated ends and emitted light with a wavelength of 694.3nm [3]. Flashlamps act as blackbody emitters, emitting broadband radiation, typically ranging from the IR into the UV range in the electromagnetic spectrum [17]. Because of their broad emission and high energy, flashlamps have been used to optically pump many different types of materials. Flashlamps immerse the material with their broad spectrum, but the material only accepts the light defined by its absorption spectra, while the rest is transformed into heat. For pumping, flashlamps are placed coplanar to the gain material and reflectors are used to image the flashlamp into the material. Generally, they are either air or water cooled, depending on the power consumption. Flashlamps are incapable of being operated at repetition rates beyond 100 Hz and pose several hazards to laser operators, such as leaked light and the high voltage necessary to ionize the internal gas.

Diode pumping has become the most predominant way to optically pump solid-state lasers, SSLs. The ability to pump at a certain wavelength, which matches with the material's absorption spectrum allows for more energy to be absorbed and used to excite atoms and less energy to go into waste [17, 18]. This, in turn, reduces the thermal stress in the solid-state gain medium, which leads to a better beam quality. With the current diode laser technologies, diodes provide an overall better efficiency (up to ten times better for Nd:YAG), a longer lifetime and safer operation [18]. Since their introduction, laser output powers have increased several orders of magnitude beyond the kW level.

### 2.1.2 Laser Resonator

By pumping the gain media, the atoms of the crystal gain energy and reach higher energy levels. Once these atoms are excited, some will spontaneously decay into a lower energy level, emitting photons. In this process called spontaneous emission, photons are emitted in all directions at random times [18]. For laser operation, the gain medium is surrounded by mirrors which reflect these photons back into the crystal. These mirrors can be used at angles to fold the laser resonator, making it possible to make complex laser cavities in a compact area. If some of the spontaneously emitted photons hit the mirrors and return the media, they are able to stimulate more atoms to produce more photons. This process is Stimulated Emission [18]. If the gain in the cavity exceeds the losses, lasing begins. Laser cavities range from simple cavities to complex multi element systems. The beam characteristics are dependent on the laser cavity design, the individual cavity elements, and the laser operational conditions in the case of thermal and non-linear effects.

As the electromagnetic (EM) wave travels through the cavity, it experiences constructive and destructive interference with the reflected EM waves. The standing waves which result from this effect are known as longitudinal modes. These modes affect the linewidth and coherence of the laser. Since the typical laser's cavity length is greater than the emitted wavelength by many orders of magnitudes, the number of modes is large [17, 18, 19]. Transverse modes represent the transverse modal distribution of a laser. These can be viewed by looking at the transverse energy distribution (beam profile) of a laser. Transverse modes

account for the beam divergence, diameter and the energy distribution of the laser beam [17, 18, 19]. The nomenclature used to describe laser modes is  $TEM_{mnq}$  or  $TEM_{plq}$ , where TEM stands for transverse electromagnetic wave; q for the longitudinal mode; and m, n, q, and l represent the number of transverse modes. The terms m and n are used for Cartesian coordinates and p and l are used for cylindrical coordinates. A Gaussian pulse is described as having a  $TEM_{00}$  mode configuration [17, 18, 19].

When a laser resonator is unstable, rays leak out of the cavity causing loss to the corresponding modes [18]. For a simple laser resonator, stability is achieved if

$$0 \leq g_1 g_2 \leq 1 \quad (2.1)$$

in which  $g_1 = 1 - \frac{L}{R_1}$  and  $g_2 = 1 - \frac{L}{R_2}$ , is satisfied [18]. This stability criterion is demonstrated in Figure 2.1, in which the shaded area represents stable resonators [18].

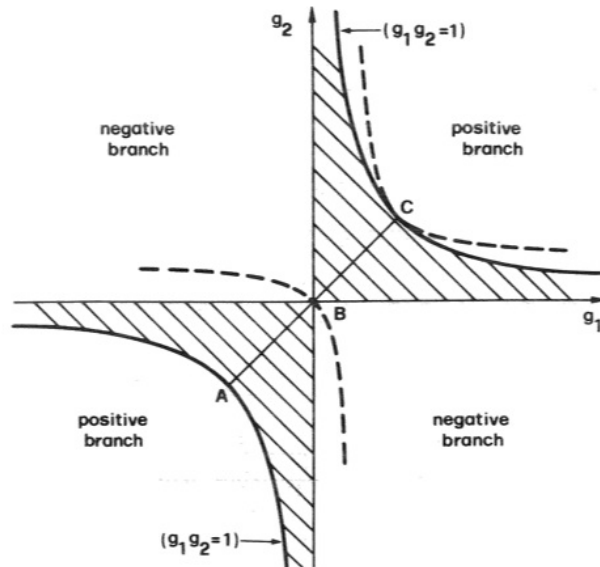


Figure 2.1: Laser Resonator Stability Criterion Plot

### 2.1.3 Pulse Generation

Generation of laser pulses commenced shortly after the invention of the laser in 1960. To produce laser pulses, the feedback of the resonator is temporarily broken, allowing the population of the higher energy level to build up. The population can be stimulated to emit of a laser pulse by restoring feedback. This produces peak powers of many orders of magnitude greater than non-pulsed lasers [20]. There are many techniques that have been used to created pulsed lasers.

#### 2.1.3.1 Q-Switching

Q-switching is a technique for creating laser pulses typically in the nano- and micro- second regime. The term itself refers to switching the quality or the losses of the laser resonator. By doing so, a large population inversion is achieved in the gain medium. There are two types of Q-switching: passive Q-switching and active Q-switching. For passive Q-switching, an element is introduced inside the laser cavity which causes the losses to increase once threshold is reached. An example of a passive Q-switching is using a saturable absorber (SA). Typical saturable absorbers consist of a dye in a solvent, a doped solid-state crystal, or a semiconductor device [19]. The SA absorbs energy from the cavity. Once the absorber saturates, it no longer absorbs and the associated optical losses decrease. This sort of

mechanism is relatively easy to implement, but the user has no control of the pulse duration or frequency of the laser pulses.

The other method for Q-switching is active Q-switching. For this, a controllable element is placed inside the laser cavity. Active Q-switching typically utilizes acoustic-optic modulators (AOM) or electro-optic modulators (EOM). The AOM works as follows: a piezo-electric transducer causes vibrations to travel through a medium, such as quartz. Once the laser is incident on the AOM, if the piezo is on, the laser itself will diffract off the acoustic wave. Typically, this diffraction is enough to break the feedback of the laser resonator. AOMs are low voltage devices that can operate over a wide range of repetition rates, but have relatively low contrast ratio of less than 100:1.

EOMs have a higher contrast and can have much faster switching times than AOMs. EOMs are based on the Pockels effect, in which a high voltage is applied, causing the non-linear crystal to become birefringent. The birefringency of the crystal is proportional to the applied voltage [18]. To create laser pulses, the birefringence of the carefully adjusted crystal causes the polarization of the incoming laser beam to change. One common implementation is to pass the beam through a PC and apply a voltage which rotates the polarization by  $90^\circ$  ( $\lambda/4$ ). If the PC is on, the beam can be expelled from the cavity by a polarizer, whereas the beam would transmit through if the PC is off.

The main problem with Q-Switched lasers is the increase in pulse duration with an increase in repetition rate. Increasing the repetition rate will decrease the pulse duration and energy stabilities. It may reach a point at which laser pulses are simply not created [21].



### 2.1.3.2 Cavity Dumping

Another type of pulse generation method is cavity dumping. This process is similar to the Q-switching method described previously and can be done with either an AOM or an EOM. Cavity dumping addresses most of the issues associated with Q-switching. By means of cavity dumping, a laser system is capable of producing laser pulses at high repetition rates with a constant pulse duration. The pulse dropout issue is eliminated for most cases. For the EOM case, the pulse duration is limited by the cavity round trip and the PC's high voltage and switching speed [22].

When the laser is cavity dumped, the laser resonator consists on HR mirrors. Because the energy is stored throughout the resonator, the system is less dependent on the material's gain than Q-switched lasers. The laser output itself is obtained by either displacing the laser pulse with an AOM onto another mirror or by using an EOM, QWP, and a polarizer to obtain the laser output through another angle of the polarizer [18, 22, 23].

### 2.1.4 Architecture

Solid State Lasers, SSLs, are described as lasers containing a gain media which has a crystalline, glass, or semiconductor based structure. After its initial demonstration, many different types of SSLs have been demonstrated, all with different host material, crystal geometry and pumping scheme. A brief explanation will be provided for the main SSL architectures.

#### 2.1.4.1 Rod Lasers

The first SSL geometry, which is still widely used in the laser development field is the rod based system. The first ruby laser had this crystal geometry. This rod geometry, in which the length is greater than the diameter, has been adapted to many different materials. Many crystals of optical quality are grown through the Czochralski method [17, 24]. By cutting apart excess material and polishing the sides, a crystal rod is obtained. Rods allow for side and end pumping techniques. However, if the rod is pumped heavily, it undergoes stress and temperature gradient dependent refractive index change that lead to thermal lensing and birefringence [17]. While this can lead to catastrophic damage, laser performance often suffers from significant beam quality degradation well below the threshold for optical damage.

#### 2.1.4.2 Slab Lasers

Further research lead to development of slab shaped host materials in 1969 [25, 26]. These have a larger surface area to pump and cool. This leads to a 1-D heat gradient in the direction of the pumping and therefore, a reduced thermal gradient normal to the beam. This reduces the biaxial focusing and depolarization losses which would occur for incoming polarized light [17]. The slab gain medium design is enhanced by cutting the facets of the crystal at Brewster's angle. By doing so, the incoming beam refracts at the crystal surface and transverses the slab through a zig-zag optical path [17]. The crystal acts as a waveguide

and the light reflects from the polished pumping edges due to total internal reflection (TIR) [26]. In the ideal case, the rectangular geometry reduces the stress induced birefringence and the zig-zag path reduces the thermal and stress induced focusing. However, the inability of maintaining the cooling constant causes thermal problems at the edges of the slab [17].

### 2.1.4.3 Fiber Lasers

The theory to produce fiber lasers was first published in 1960, with the demonstration of the first fiber lasers soon after [27]. These first fiber lasers were doped with neodymium (Nd). Fiber lasers consist of a glass host doped with rare earth ions in the gain media. Effectively, fiber lasers are simply rod lasers with extremely high length to diameter ratios. With proper waveguide engineering, both signal and pump beams propagate in confined areas with high overlap, leading to highly efficient pumping. Generally, mirrors are used to reflect the light back into the cavity, but sometimes the Fresnel reflections from the facets of the fiber are enough to cause lasing. Given the flexibility of the fibers and the pumping schemes, these can be cooled very efficiently and uniformly. Fiber lasers can provide very good beam qualities at high continuous powers; however, high energy fiber lasers are difficult to achieve, since the small core area leads to very high laser intensity which can induce nonlinear effects or cause optical damage, even at modest energies.

#### 2.1.4.4 Active Mirror Lasers

The active mirror laser was invented the late 1960's [28]. This type of laser consists of a gain disk whose back coating permits pump light and prevents laser light transmission and also incorporates an antireflective (AR) coated front face [17]. This setup allows for the uniform and efficient pumping and extraction of laser light. This scheme and provides a high surface area to volume ratio providing improved heat removal and diminished thermal distortions [17]. This architecture is the basis for the thin disk laser.

#### 2.1.4.5 Thin Disk Lasers

The thin disk laser was first demonstrated by Giesen et al. in 1993 [16, 22]. Giesen's group sought a way to handle the thermal stresses in a laser in a more efficient manner. The concept behind this idea was to use a gain medium that would be thin enough to reduce the heat problems that often lead to thermally induced lensing within the gain media. The drawback of the design was the loss in gain due to the smaller amount of ions interacting with the pump light. The solution to this problem was to introduce a multiple pass absorption technique, in which the same pump light would travel through the medium multiple times [29]. Yb:YAG was chosen as the gain medium for the thin disk laser due to its small quantum defect, high thermal conductivity and mechanical strength, and the ability to heavily dope

Yb to increase absorption. The rest of this chapter reviews thoroughly the main concepts behind the thin disk laser technology.

## 2.2 Gain Media

### 2.2.1 Gain Requirements

Thin disk lasers depend on a very thin disk to achieve large gain. For efficient laser operation, strong absorption is desired. However, the small thickness limits the pump absorption and laser gain achievable in a single pass through a disk.

There are many different types of media that have been adapted to the thin disk design. These include materials such as Yb:YAG [16], Nd:YAG [30], Nd:YVO<sub>4</sub> [31], Tm:YAG [32], Yb:KYW [33], and other crystals, typically doped with Yb. Even though a large range of materials have been explored for thin disks, Yb:YAG still predominates. Yb:YAG has very interesting characteristics that make it the ideal candidate for a thin disk. These characteristics will be discussed in detail in the following sections.

## 2.2.2 Yb:YAG

### 2.2.2.1 Energy Levels

The energy of a molecule is the summation of four different types of energy: electronic, rotational, vibrational, and translational. All of these, except for the translational energy contribute to possible laser action [18]. Following the Born-Oppenheimer approximation, it has been demonstrated that electronic, rotational, and vibrational transitions account for emissions from the UV to near-IR (up to  $1\mu\text{m}$ ), where as vibrational and rotational account for Mid-IR emissions and pure rotational transitions account for Far-IR emissions [18, 34].

To get laser action, atoms which are originally in the ground state are pumped to reach a higher energy level. Population inversion, a requirement for laser operation, is reached when there is a higher population of ions in the upperstate than in the lower state. Naturally, these atoms have a tendency to lose energy by non-radiative (thermal) transitions or by spontaneously emitting light. The rate at which ions are excited must exceed the rate of relaxation to maintain population inversion.

Lasers are described as having 3, quasi-3, and 4 energy level systems. A diagram of the energy level systems is illustrated in Figure 2.2. A 3-level system is composed of the following levels: the ground state, an upper state, and a relaxed state where electrons decay from the upper state by means of thermal transitions. Emission of light, whether spontaneous or stimulated, occurs between the relaxed and ground state. The thermal transitions are faster

than the radiative decay. The 4-level system has a similar setup to the 3-level system, with the addition of a relaxed state above the ground state. In this system, an ion is pumped to an upper excited state, from which it decays non-radiatively to an intermediary upper laser level and eventually energy is released in the form of photons. After this radiative transition, the ion is in the laser level, from which it decays to the ground state. When the ion reaches the ground state, it can be excited again. The quasi-3-level system is similar to the 4-level system but the lower laser level overlaps with the ground level. 3 level and quasi-3 level systems suffer from reabsorption, in which an emitted laser photon is absorbed by an atom in the lower laser level at thermal equilibrium. This increases the threshold power required for population inversion [21, 35].

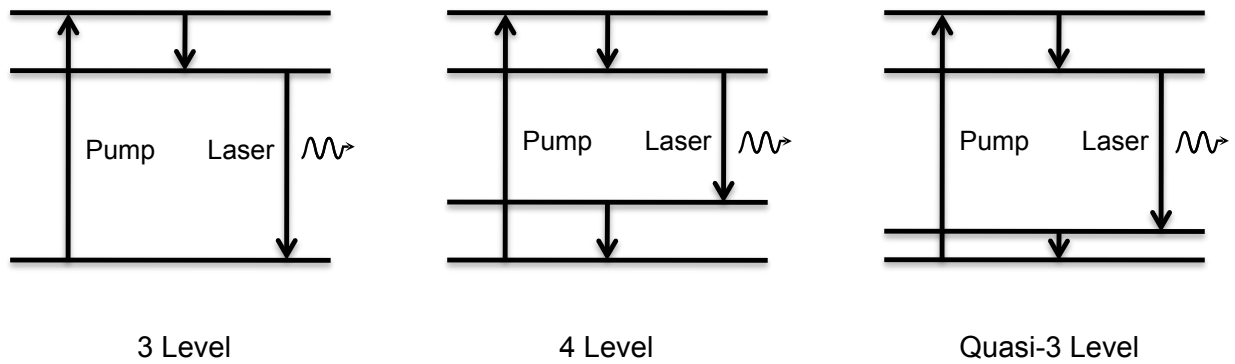


Figure 2.2: Energy Levels

The energy levels for Yb:YAG can be seen in Figure 2.3. The picture shows the two main energy level manifolds: the ground state,  $^2F_{7/2}$ , and the excited state,  $^2F_{5/2}$  [24, 35]. The upward arrows between the energy level manifolds represent the peak absorption lines and the arrows pointing down represent the peak emission lines.

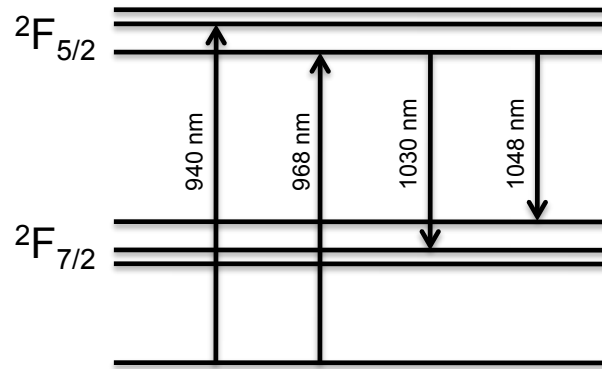


Figure 2.3: Yb:YAG Energy Levels

### 2.2.2.2 Upper-State Lifetime

The upper-state lifetime of the gain medium corresponds to the time the electron remains at the upper energy state prior to its spontaneous decay. For laser action, a long upper-state lifetime makes it easier to achieve population inversion and allows the material to store more energy for pulsed applications[17, 19]. Generally, rare-earth doped media have relatively long upper-state lifetimes [21]. For example, the upper-state lifetimes for Nd:YAG, Yb:YAG, and Tm:YAG are 230, 960, and 10000  $\mu s$ , respectively. In contrast, the upper-state lifetime of well known media doped with heavy metals, such as titanium doped sapphire (Ti:sapphire) and chromium doped lithium strontium aluminum fluoride (Cr:LiSAF) tend to be shorter (3.2 and 67  $\mu s$ , respectively) [36]



### 2.2.2.3 Absorption and Emission

Absorption occurs when the atoms of the crystal are in the ground state and are optically pumped. The manifolds corresponding to the ground state ( $^2F_{7/2}$ ) and upper state ( $^2F_{5/2}$ ) were discussed in Section 2.4.2.1. The absorption spectrum for Yb:YAG is shown in Figure 2.4.a [37]. The diagram shows that Yb:YAG has absorption peaks at 941 and 968 nm, which can be effectively pumped using an InGaAs laser diode. As previously mentioned in Section 2.1.1, the diode's spectrum is temperature dependent. The 18 nm absorption line at 941 nm facilitates diode pumping for a range of diode temperatures [24].

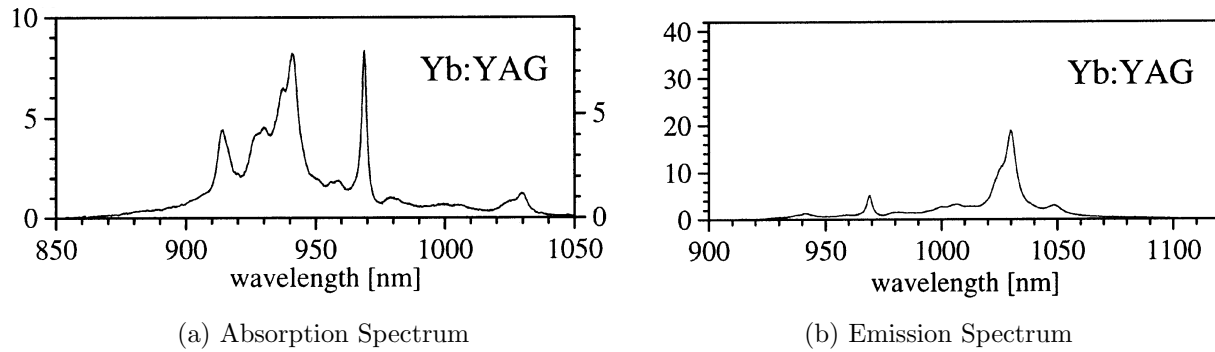


Figure 2.4: Yb:YAG Cross Section Spectra

Emission occurs when an atoms decays to a lower energy level and releases a photon. The photon released has a lower energy than that of the pumping photons, hence a longer wavelength. For spontaneous emission, these photons will emit at random times and directions. Once the media is inside a laser resonator and spontaneous emission has created some photons, the photons will stimulate more ions to emit photons coherently. The emission spectrum for Yb:YAG can be seen in Figure 2.4b [37]. Yb:YAG has emission peaks at 1030

and 1048 nm, with the dominant emission being at 1030 nm. The width of the main emission peak at full width at half maximum (FWHM) is 6 nm [36].

#### 2.2.2.4 Quantum Efficiency

Quantum efficiency (QE) is a measure of the amount of energy that is transferred from the pump photons to the laser photons [18]. A high QE is essential for an efficient laser.

Quantum efficiency is defined as:

$$\eta_q = \frac{h\nu_l}{h\nu_p} = \frac{\lambda_p}{\lambda_l} \quad (2.2)$$

where  $h$  is Planck's constant,  $\nu_l$  and  $\lambda_l$  are the frequency and wavelength of the laser respectively, and  $\nu_p$  and  $\lambda_p$  are the frequency and wavelength of the pump source. Using Equation 2.2 [18], the quantum efficiency for a Yb:YAG laser being pumped at 941 nm and lasing at 1030 nm is approximately 91.4%.

#### 2.2.2.5 Quantum Defect

Quantum defect (QD) is a measure of the energy difference between the pump and the laser emission [21]. A low QD denotes that less energy is being lost due to heat transitions and other mechanisms [18]. The quantum defect for an Yb:YAG laser can be calculated using

Equation 2.3 yielding 8.64%.

$$q = \frac{h\nu_p - h\nu_l}{h\nu_p} = 1 - \frac{\lambda_p}{\lambda_l} \quad (2.3)$$

### 2.2.2.6 Doping

For Yb:YAG, ytterbium ( $\text{Yb}^{3+}$ ) ions replace yttrium ions ( $\text{Y}^{3+}$ ) in yttrium aluminum garnate ( $\text{Y}_3\text{Al}_5\text{O}_{12}$ ). Due to Yb and Y having similar atomic sizes, the concentration of Yb can be particularly high without significantly reducing crystal quality. For Nd:YAG, the larger neodymium ( $\text{Nd}^{3+}$ ) atoms replace  $\text{Y}^{3+}$ , preventing the growth of optical quality crystals with dopant concentration greater than 1.5 at.% [38]. Yb:YAG can be doped up to 30 at.% (atomic percentage) without suffering from doping quenching [24]. Reports of up to 50 at.% doping for Yb:YAG crystals grown through the Czochralski method have been reported by Xu, et al. These crystals suffered concentration quenching, which caused the fluorescence lifetime to decrease [39]. In contrast, Nd:YAG suffers from this type of quenching past 1.5 at.% doping [21]. A relatively high doping concentration is essential to achieve gain in a thin disk due to the limited pumping volume. Typical Yb:YAG thin disk lasers operate with doping concentrations of 9-11 at.%. A thin disk laser with a concentration of 19 at.% was successfully demonstrated by Giesen, et al. [29].

### 2.2.2.7 Cross Sections

Stimulated emission cross section ( $\sigma_e$ ) is a measure of the probability that a stimulated emission transition will occur [18]. This cross section decreases with increasing media temperature, leading to the concept of cryogenically cooling gain media to obtain a high stimulated emission cross section [24]. At room temperature, the typical stimulated emission cross section for Yb:YAG is  $2.1 \times 10^{-20} \text{ cm}^2$  for the laser wavelength of 1030nm [40].

Similarly, absorption cross section ( $\sigma_a$ ) is a measure of the probability that absorption will occur [18]. As the doping concentration increases, the absorption cross section increases. For the pump wavelength, 11 at.% doped Yb:YAG's absorption cross section is  $0.77 \times 10^{-20} \text{ cm}^2$  [40]. As compared to other compounds, Yb:YAG's CS's are relatively small; therefore, a multiple absorption process is used to compensate for the small gain.

### 2.2.2.8 Comparison to Other Gain Media

The most commonly used gain media used to date for solid-state lasers is Nd:YAG, because it is easy to grow and very efficient for flash lamp and diode pumping. Nd:YAG provides a lower threshold than Yb:YAG, making it easier to obtain stimulated emission with low power pumping. As compared to Yb:YAG, its crystal structure is similar since they are based on YAG, but it does not allow for as high a dopant concentration.

Nd:YVO<sub>4</sub> is very similar to Nd:YAG, especially in operating wavelengths. The main reason why Nd:YVO<sub>4</sub> is not as widely used is the difficulty in growing large crystals that are suitable to make large gain media. It also has worse thermal conductivity and a lower damage threshold. However, Nd:YVO<sub>4</sub> has greater cross sections than Nd:YAG, thus it experiences a higher gain. It also has a shorter upper state lifetime than both Yb:YAG and Nd:YAG, so the peaks produced by Q-switching have lower energies, but potentially have a smaller pulse duration [21].

A comparison of the different types of gain media which were mentioned previously is summarized in Table 2.1 [17, 18, 36, 40, 41].

Table 2.1: Comparison of Different Thin Disk Laser Gain Media's Characteristics at Room Temperature

Medium	Yb:YAG	Nd:YAG	Nd:YVO <sub>4</sub>	Tm:YAG	Yb:KYW
Emission Wavelength (nm)	1030	1064	1064	2020	1025
Absorption Wavelength (nm)	941	807.5	808.5	785	981
Quantum Defect (%)	8.64	24.11	24.01	61.1	4.3
Quantum Efficiency (%)	91.4	78.4	78.5	38.9	95.7
Energy Level Type	Quasi-3	4	4	3	Quasi-3
Upper-State Lifetime ( $\mu$ s)	960	230	98	10000	600
Absorption CS ( $10^{-20}$ cm <sup>2</sup> )	0.77	67	114	0.48	13.3
Emission CS ( $10^{-20}$ cm <sup>2</sup> )	2.1	28	250	0.22	3
Linewidth (nm)	6	0.45	0.8	400	16

## 2.3 Technology

Thin disk lasers are generally very efficient and less prone to problems due to high power or temperature and demonstrate good power scalability and stable laser output. This section provides detailed information for several aspects of thin disk laser architecture.

### 2.3.1 Thermal Management

One of the main problems related to temperature within a gain medium is thermal lensing. This phenomenon occurs when a temperature gradient is formed within the medium due to pumping, changing in the index of refraction of the material [42]. Efficiently cooling the gain medium helps reduce thermal lensing, but it is not sufficient, since pumping and cooling are done simultaneously. Thermal lensing can disturb cavity stability and reduce efficiency and beam quality. Rod based lasers use a two dimensional heat conduction mechanism, producing a parabolic thermal gradient. However, thin disk lasers use a one dimensional heat conduction mechanism, producing a flat temperature profile [42].

Overheating can also damage intra-cavity optics and coatings. This is especially true in media with a large quantum defect, in which a large amount of energy is converted into heat [18]. If the gain medium is able to be maintained below a certain temperature to avoid most of the thermal effects, then the output power of the laser is proportional to the pump area [42]. Such is the case for most thin disk lasers.

### 2.3.1.1 Cooling Finger

For thin disk lasers, the medium is maintained at a specific temperature by soldering the disk to a copper heat sink. The disk is soldered using indium or gold-tin foil [43, 44]. A coolant is pumped at a constant rate extracting the heat from the heat sink. By attaching the gain medium to the heat sink, a one dimensional heat flux is maintained within the crystal [29]. Maintaining the disk at a semi constant temperature allows for higher pumping powers. The cooling apparatus which holds the thin disk is referred to as the cooling finger. Figure 2.5 shows a simple linear cavity configuration with the cooling finger apparatus.

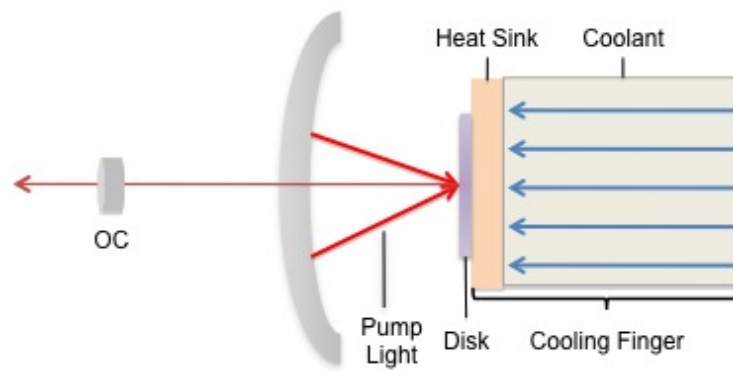


Figure 2.5: Thin Disk Cooling Configuration

Ehard et al. demonstrated that for thin disk lasers, the optical efficiency increases with a decrease in temperature [45]. Temperature dependent laser models indicate that Yb:YAG will work very efficiently at cryogenic temperatures [24]. Yb:YAG operates as a 4-level system at cryogenic temperatures, allowing efficient operation with relatively low power diodes due to the diminished laser wavelength reabsorption.

## 2.3.2 Pumping

Diode laser are used to pump thin disk lasers. The pumping configuration is different from other lasers, due to the geometry and size of the disk. This section discusses in detail the different pumping mechanisms used for thin disk lasers.

### 2.3.2.1 Multi-Pass Absorption

The geometry of thin disk lasers required an innovative and effective pumping scheme that took into consideration the absorption of a very thin laser gain medium. To produce population inversion, Giesen's et al. demonstrated an 8-pass absorption technique. A parabolic mirror is used to image the pump light onto a disk, which is located at the focal position of a mirror. The pump radiation transverses the disk and reflects from a HR coating on the back of the disk [29]. The remaining pump light reaches the parabolic mirror and is reflected back onto the disk to repeat the process.

The initial design was later revised and the number of absorption passes increased from eight up to 32 by means of using multiple roof prisms (generally three) and a retroreflector. The roof prisms deviate the pump light which remained after the initial reflections and allows it to repeat the absorption cycle [46]. Multiple absorption passes allows for a decreased doping concentration or disk thickness. Also, by having multiple absorption passes, the power density increases, thus decreasing the threshold power [29]. Even after multiple passes, there



is still some remaining pump light which is reflected back into the pump diodes, but it is low in power, so no damage is done to the diodes. The multi-pass absorption scheme can be seen in Figure 2.6. The number of passes have been reduced in the image for ease of understanding. Figure 2.6.b shows the multiple absorption passes on the parabolic mirror. Introducing a mirror after the last pass doubles the amount of passes encountered by the disk [46].

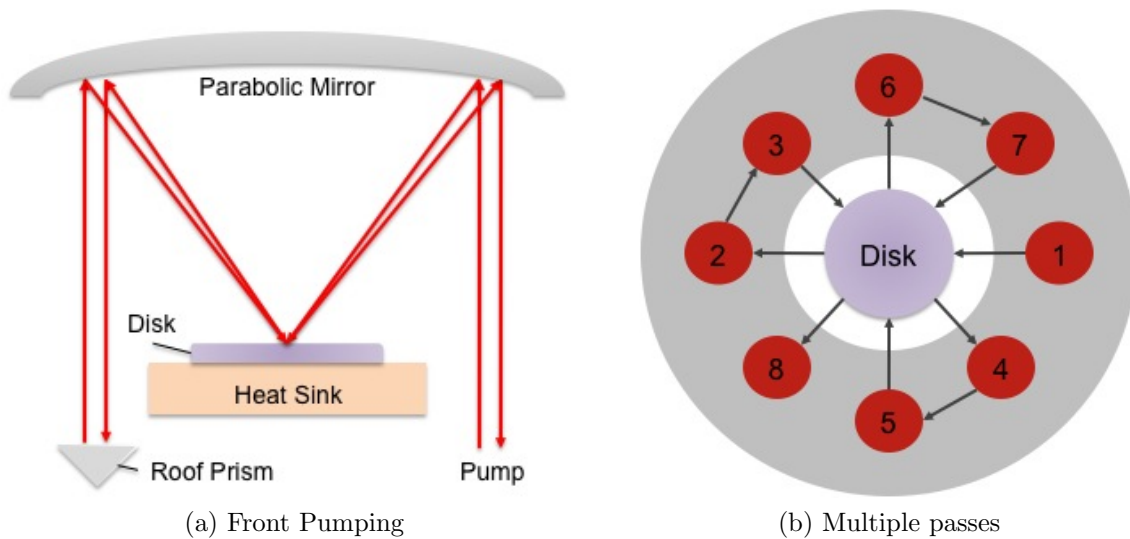


Figure 2.6: Thin Disk Multiple Pass Pumping

### 2.3.2.2 Side Pumping

Side or edge pumping has been demonstrated as another efficient method of pumping high power thin disk lasers. Absorption of up to 100% is achievable using this technique. For this pumping mechanism, the disk has a central doped region and an exterior undoped region,

which acts as a waveguide for incoming pump radiation and dampens generation of amplified spontaneous emission (ASE) [45]. This geometry is harder to produce and does not produce a one dimensional heat flow, which leads to possible thermally induced problems.

### **2.3.2.3 Disk Coatings**

To diminish optical losses, the disk has multilayer dielectric AR and HR coatings for both 940 nm and 1030 nm. The AR coating is located in front of the disk, where the light is incident on the disk. The HR coating is located on the back of the disk, before the heat sink, and acts like a mirror for both the pump and laser wavelengths.

### **2.3.2.4 High Power Pumping**

To obtain higher powers from thin disk lasers without exceeding the damage threshold requires increasing the pump spot area and the laser diameter on the disk. However, changing this pumping area also affects the beam quality of the laser [42]. To obtain very large powers from a single disk, a large diameter disk is required. This is the case for multi-kilowatt thin disk lasers using only multiple high power pumps to power one disk. For example, multi-kilowatt systems (4 kW) using one disk with up to six laser diodes are being produced by TRUMPF Laser GmbH. Typically disk diameters range from 10 to 20 mm, depending on the required power [47].

### 2.3.3 Laser Resonator

A linear cavity can be formed by placing an output coupler (OC) in front of the disk. Similarly, a V-shaped cavity can also be made by placing a HR mirror and an OC on each arm with the disk at the vertex. The V-cavity provides more space for intracavity optics. By increasing the cavity length, a higher beam quality can be achieved, with a loss in efficiency [48]. The length can be increased while maintaining a small footprint by using a V-shaped cavity. Using other cavity shapes allow for multiple intracavity optics and thin disks to be introduced. A simple linear cavity was demonstrated in Figure 2.5.

## CHAPTER 3

### TRUMPF TRUMICRO 7050 SETUP

This chapter introduces the Trumpf TruMicro 7050 obtained by the EUV group.

#### 3.1 Cavity Design

The cavity layout for the TruMicro 7050 is shown in Figure 3.1. The laser cavity has three HR flat mirrors, a thin-film polarizer at Brewster angle, a Pockels cell and quarter wave plate for cavity dumping, and the disk with the pumping optics. The laser outputs through the polarizer and is diverted by two mirrors located at the left of Figure 3.1. The system also has several additional components non included in the layout drawing. Figure 3.2 is a photo of the actual laser cavity.

#### 3.2 Pumping Scheme

The TruMicro 7050 uses two laser diodes which can generate up to 1.25 kW of optical power each at 940 nm. The diodes are attached to a base, which is connected to the main laser breadboard. The light output is fed to the enclosure area through several optics within

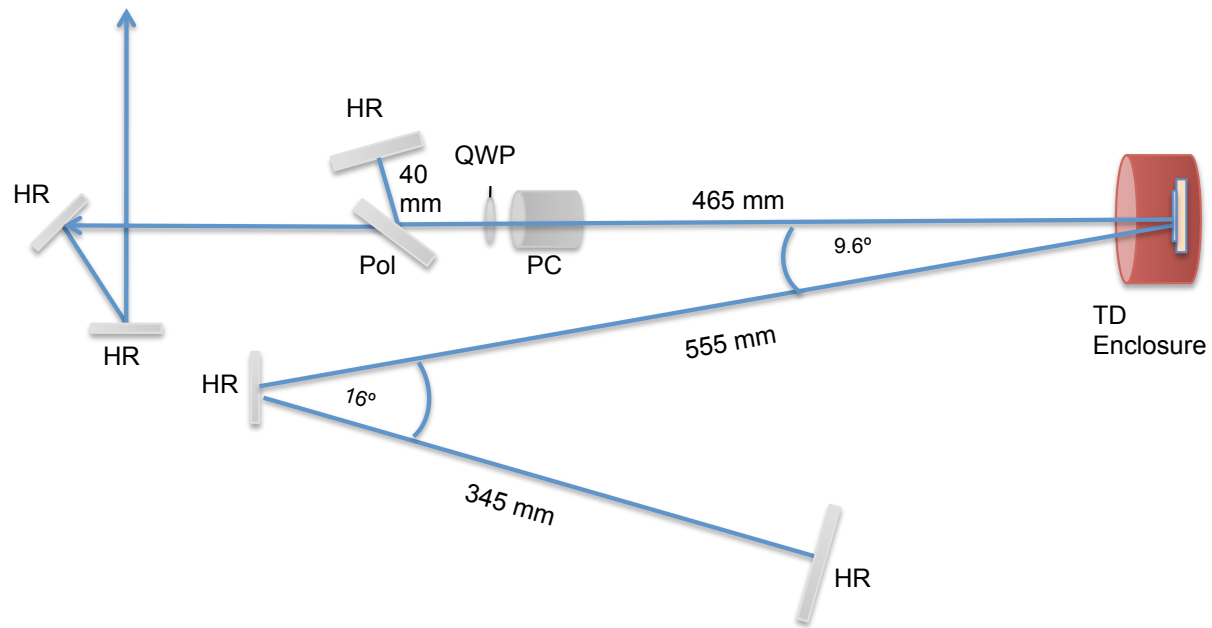
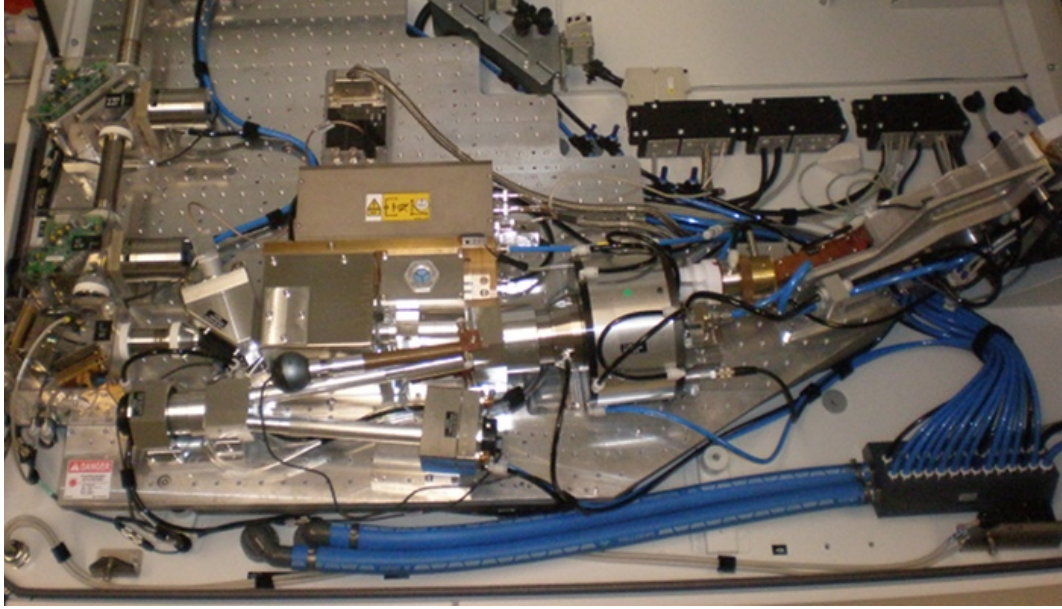


Figure 3.1: Trumpf TruMicro 7050 Cavity Layout

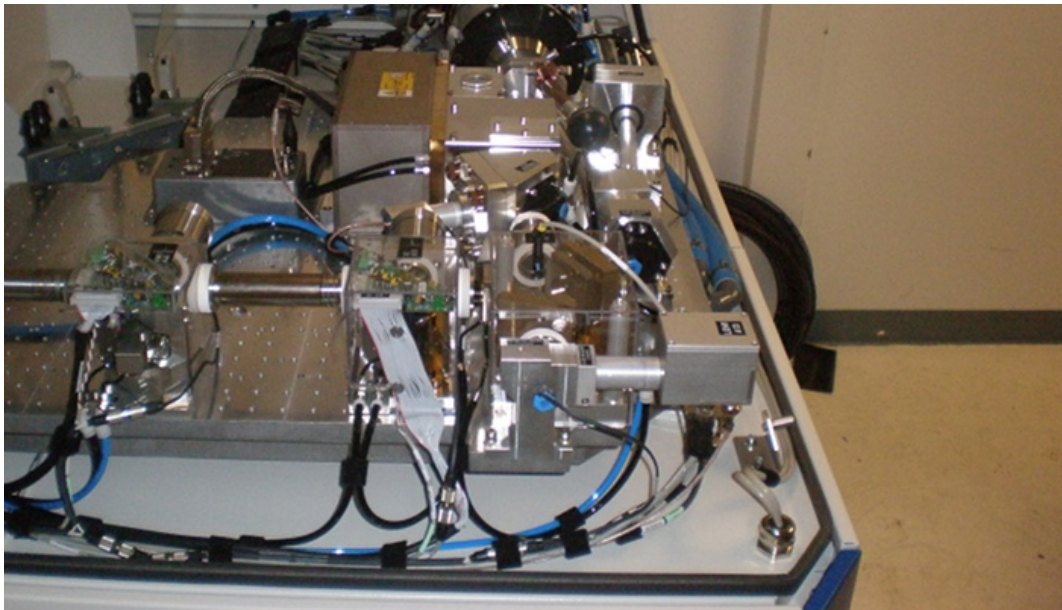
the diode mounting base. The optics homogenize and collimate the pump laser beam. A parabolic mirror is used to image the pump onto the disk. The pump beam has a diameter of 6.3 mm at the disk interface. By means of a prisms and the parabolic mirror, the disk encounters 16 absorption passes. The laser diodes and base can be seen in Figure 3.3.

### 3.3 Thin Disk Design

The Trumpf TruMicro 7050 uses a 14 mm diameter Yb:YAG thin disk as its gain medium. The information regarding the thickness and doping concentration of such disk is proprietary to Trumpf Laser GmbH. The disk itself has a slight curvature of 1 diopter (focal length of 1 m). When the disk is pumped, there is a slight deformation to this curvature. Figure 3.4



(a) Cavity Top View

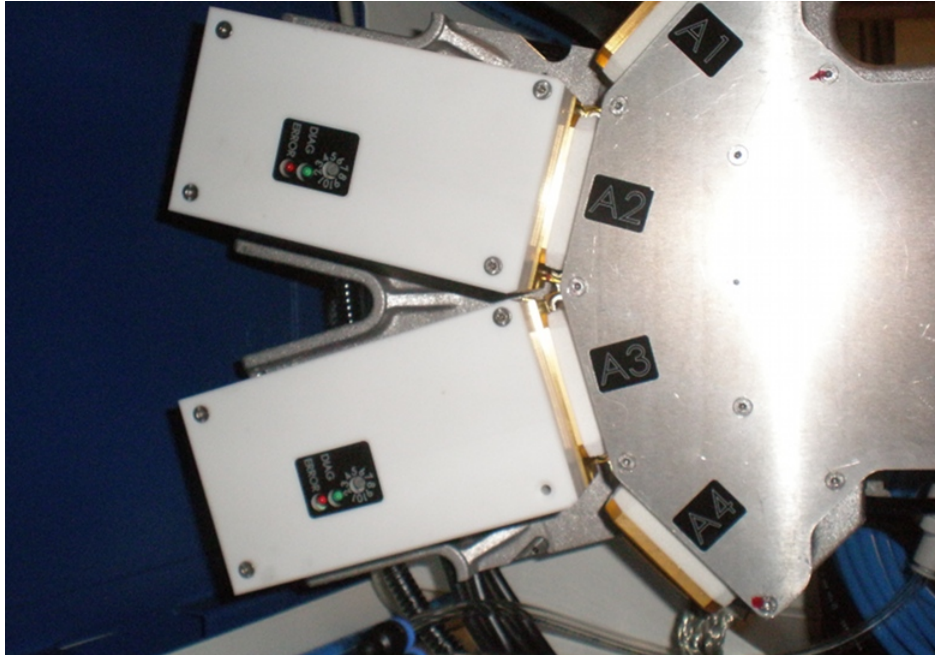


(b) Cavity Side View

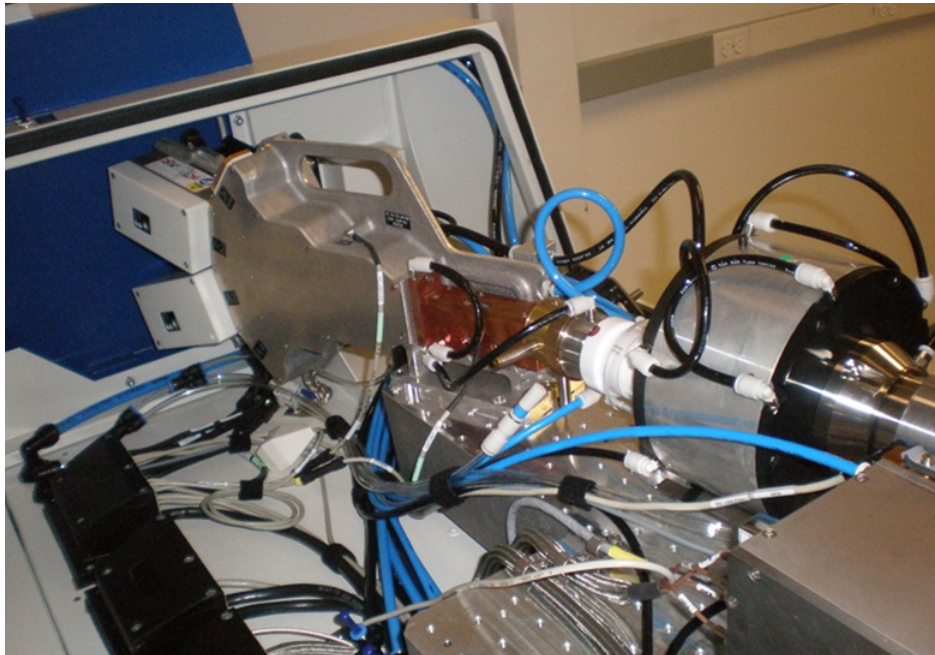
Figure 3.2: Trumpf TruMicro 7050 Laser Cavity

shows the fluorescence of the disk when feedback is broken and when it is permitted in the system.





(a) Laser Diodes



(b) Diodes Attached to Base

Figure 3.3: Trumpf TruMicro 7050 Pump Laser Diodes

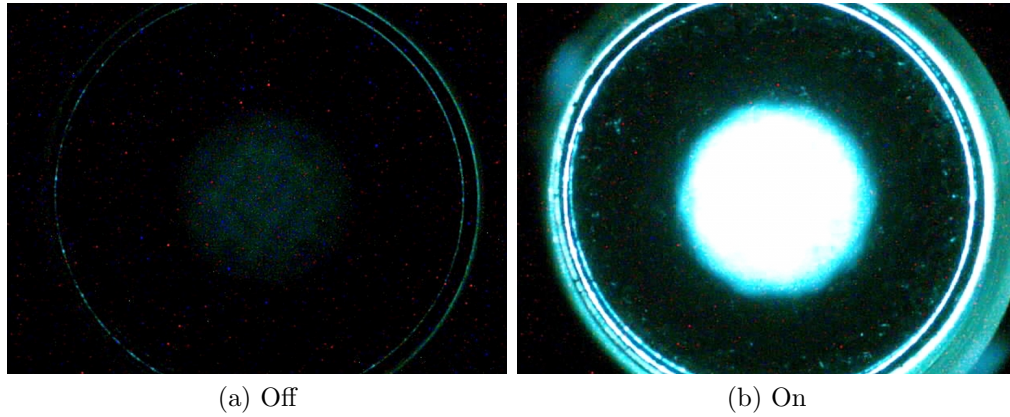


Figure 3.4: Trumpf TruMicro 7050 Disk Fluorescence

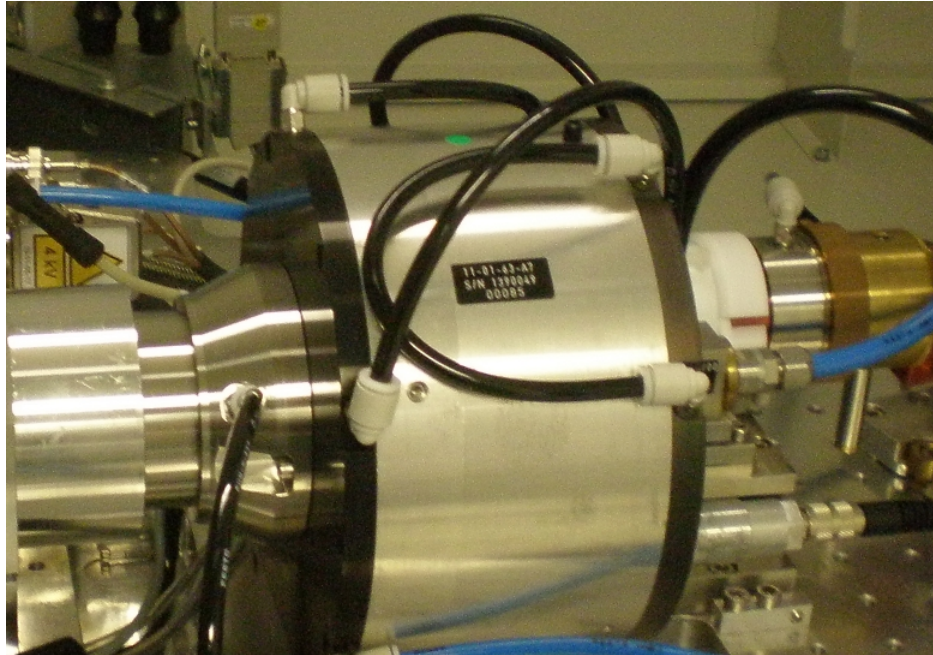
### 3.3.1 Disk Enclosure

The thin disk is enclosed within a protective structure. This enclosure holds the parabolic mirror which reflects the pump light onto the disk surface and the optics used to increase the amount of absorption passes. The enclosure has 3 main openings at the back, allowing for the insertion of the cooling finger with the mounted disk, the pump light optics, and a sensor. On the front, there are four main apertures, two of which are for the cavity arms, one for a charge-coupled device to view the disk and one for a disk fluorescence sensor. The enclosure structure along with some of the connections can be seen in Figure 3.5.

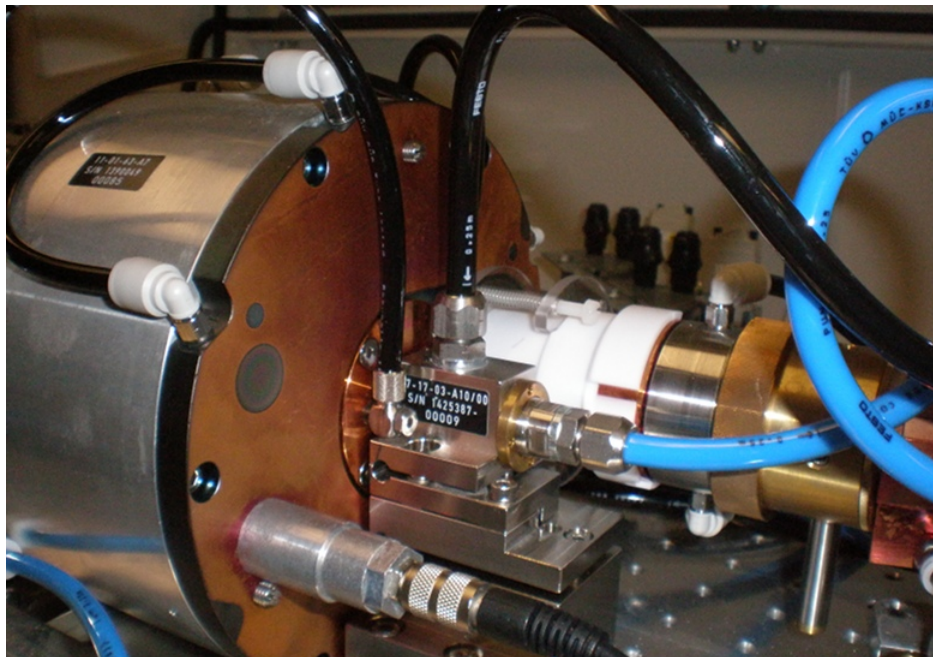
### 3.3.2 Cooling Finger

The cooling finger that holds the disk and the heat sink within the enclosure is showed in Figure 3.5b. At the opposite end of the disk, cold water is sprayed against the heat sink to





(a) Laser Diodes



(b) Diodes Attached to Base

Figure 3.5: Trumpf TruMicro 7050 Pump Laser Diodes

remove heat and returns through the water connection on top of the module. The cooling finger allows for slight orientation displacement for alignment purposes.

## 3.4 Pulse Generation

### 3.4.1 Cavity Dumping

The TruMicro 7050 generates laser pulses by employing cavity dumping. The laser cavity uses a Pockels cell (PC) as the optical modulator. Figure 3.6 shows a sample cavity dumping timing diagram including the PC trigger (square pulse), the intracavity pulse (dashed line) and the output pulse (solid line). The configuration is such that the PC affects only part of the intracavity laser pulse. The PC is turned on at the time that the peak of the pulse interacts within the PC. This changes the polarization of the second half of the pulse. The last section of the pulse transmits through the polarizer, while the rest remains in the cavity. Since not all of the energy is expelled as in a standard Q-switched laser, the intracavity intensity is maintained at a high value. Changing the voltage on the PC affects the polarization, which changes the transmission at the polarizer and, in turn, affects the rise time of the pulse leaving the resonator [49]. For this reason, the minimum pulse duration is achieved at the highest voltage allowed for the system, corresponding to near  $\lambda/4$  voltage on the PC [22].

A square wave is used to drive the PC. When the trigger signal is high, the PC is off; therefore, the polarizer reflectivity is near 100%, so most of the light remains within the cavity. When the signal is low, the polarization can be varied to expel the laser pulse. The period of the high voltage signal can be varied to select the pulse repetition rate (from 5-100 kHz), and the level can be tweaked to adjust the pulse duration [49].

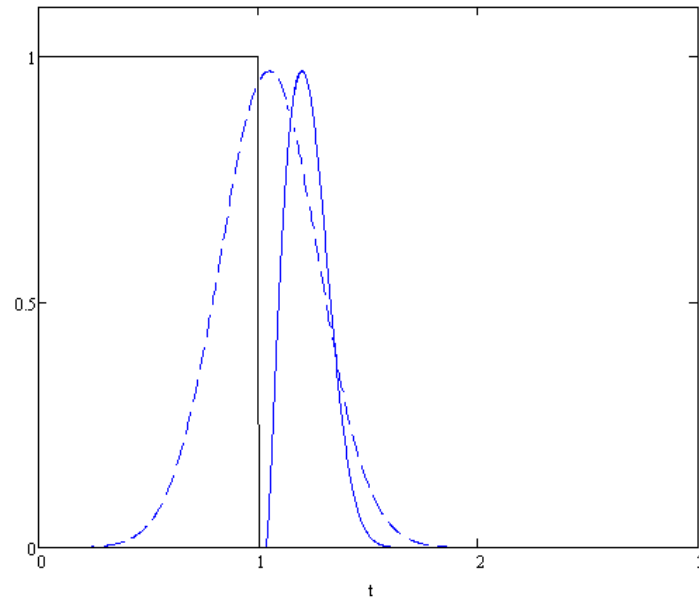


Figure 3.6: Trumpf TruMicro 7050 Cavity Dumping Timing Diagram

For CW operation, HV is always applied to the PC, whereas this voltage is modulated in the pulsed regime. To reduce the risk of laser pulse instabilities, the laser is always kept above lasing threshold.

### 3.4.1.1 Optoelectronics

The TruMicro 7050 uses a 10x10 mm<sup>2</sup> beta barium borate (BBO) crystal as the Pockels medium. A high voltage signal is applied to the PC to cause a polarization rotation on the incoming laser EM wave. Due to the dimensions of the crystal, it requires a current of ~100 mA to rotate the polarization. At such a high voltage, this current is potentially fatal. The PC is EM shielded and an interlock prevents a HV discharge if the shield is removed. The BBO has AR coated windows and is in a dry enclosure. Dry air is pumped to remove any moisture from the cavity and PC optics. Chilled water is pumped through the PC to remove any heat. Figure 3.6 shows the TruMicro 7050 Pockels Cell.

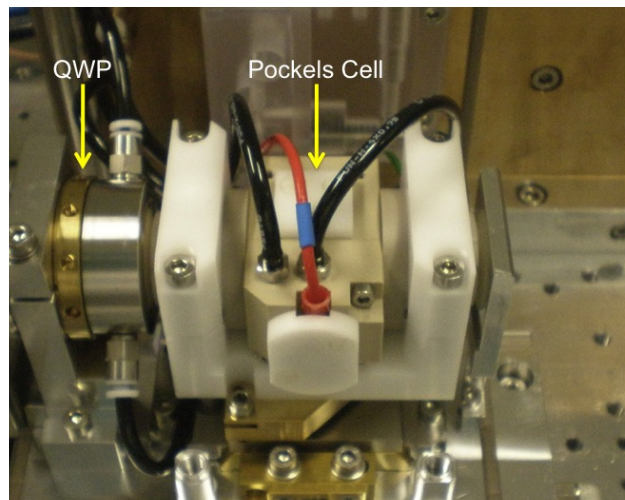


Figure 3.7: Trumpf TruMicro 7050 Pockels Cell

A QWP is used to adjust the transmission through the polarizer [22]. This allows for the laser to operate in CW mode when the PC is off. The QWP can be easily rotated to tweak the laser pulse to the desired conditions. The PC would require a substantial greater

HV in order to produce half wave ( $\lambda/2$ ) rotation (up to 10.8 kV). Operation at such a high voltage can produce electrical arcing. The QWP induces a phase retardation of  $\pi/2$  ( $\lambda/4$ ) on the intracavity laser light, reducing the required HV applied to the PC to achieve half wave rotation.

The cavity has a thin film polarizer (TFP) at Brewster angle, which acts as the output coupler. When the PC is off, the TFP is highly reflective; therefore, no light is coupled out.

#### **3.4.1.2 Energy Sensor**

The TruMicro has a calibrated photodiode located behind the HR mirror next to the polarizer. This sensor, once calibrated, is able to detect the intracavity power and provide feedback in order to control the level of amplification of the gain. This sensor is essential when the laser is ran in pulsed mode. When pumped and not controlled, Yb:YAG's long upperstate lifetime can lead to chaotic pulse behavior. The chaotic behavior or too much intracavity power can cause damage to the resonator optics. The sensor was calibrated with the help of the Trumpf scientists in order to ensure safe and regular pulsed operation.

## 3.5 System Design

The Trumpf TruMicro 7050 is a self contained system, requiring only a supply of electricity and chilled water. These requirements and the different systems will be discussed within this section.

### 3.5.1 Electrical System

The laser system has a requirement of 5 kW input power for optimum operation. It is able to operate under the following conditions:  $380 \leq V \leq 460$ ,  $50 \leq Hz \leq 60$  [50]. The 3-phase voltage is in wye configuration within the laser system and thus requires around 12A for stable operation. This input power is sufficient to power all of the demanding components of the laser including the water pumps, air compressor, main computer, Pockels cell driver, pump laser diodes, and others. The system has a wall-plug efficiency of 20%.

### 3.5.2 Control System

The TruMicro 7050 has a built in central processing unit for systems management. It is able to monitor the water and air pressure throughout the system, electrical power, any scattering of light, and other anomalies that could lead to damage within the system and shut down

if necessary. Calibrated diodes and sensors throughout the laser cavity provide the system with feedback related to laser operation.

The CPU itself can be accessed and operated by means of the laser remote or an externally interfaced computer. These provide the user with detailed information and diagrams that promote a safe working condition. It also includes a detailed list of possible and past errors associated with the laser.

### **3.5.3 Thermal Management**

The Trumpf laser has a closed loop cooling system using chilled deionized (DI) water. There are particle filters and deionizers in place to make sure all the water within the laser is clean and ion free. An external chilled water supply is necessary to chill the DI water within the laser. At full power, the chiller has a heat load of up to 5.8 kW and must maintain a temperature between 5°C and 22°C [50]. This chilled water is capable of removing more than the heat load from this laser. Filters were placed in parallel before the laser in the supply line to minimize the amount of debris that reached the laser.

### **3.5.4 Humidity Control System**

The TruMicro 7050 also has an air cleaner and compressor system. The system cleans the air, dehumidifies it, and distributes it throughout the laser cavity. This is crucial to the laser

because any moisture or particles inside of the laser cavity can cause damage. The filters in place for this system have a lifetime of 5000 hours. The whole air cleaner unit has to be replaced every 10000 hours [51]. To promote a clean environment for the laser, the EUV lab is operated as a clean room with HEPA filtration.



## CHAPTER 4

### LASER CHARACTERIZATION

The TruMicro 7050 is a versatile system allowing for different operation modes. It yields up to 808 W in continuous wave (CW) mode and can provide up to 80 mJ in pulsed mode. Many of the laser parameters can be tweaked to meet certain criteria; however, the amount of tweaking for some parameters is limited due to the potential of damaging the optics due to very high intracavity powers.

#### 4.1 Continuous Wave Operation

The initial laser cavity setup consisted of a 91% OC situated after the polarizer. With this configuration, the laser was able to produce up to 1.31 kW of CW laser light at 100% of pumping power. To cavity dump the system, a QWP and a PC were placed within the cavity and the 91% OC was replaced with an HR mirror. This new setup was also characterized, yielding up to 880 W at 70% of pumping power. Any further increments of the pump laser diodes could damage the optics.

In order to measure the power output, a multi-kW thermal detector was placed at the end of the laser. A negative lens was placed to expand the beam so as to diminish the probability

of damaging the detector. The power output of the laser grew linearly with power. This power scalability is observed in thin disk lasers due to the lower ratio of pump power being converted into thermal energy. The slope efficiency for the laser is shown in Figure 4.1. The plot compares the efficiencies prior to and after the 91% OC change and the PC and QWP insertion. For the 91% OC configuration, the slope efficiency was 66% and for the HR setup, the efficiency was 62%.

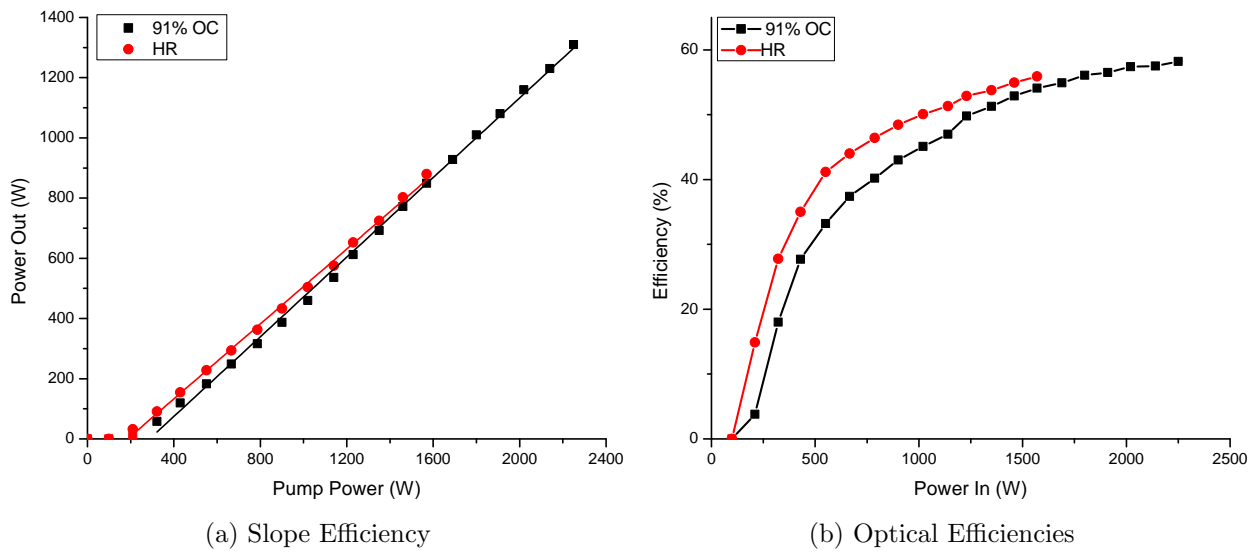


Figure 4.1: Trupf TruMicro 7050 CW Efficiencies

#### 4.1.1 Intracavity Power

To quantify the intracavity power, a sensor was placed after the last cavity mirror. This small photodiode detects very small amounts of light that leaks from the mirror. The diode was calibrated in order to obtain accurate measurements. The calibration was done with the cavity dumping setup, but the last HR mirror was replaced with a 91% OC. Replacing the

mirror ensured less light would lase through the polarizer, leading to more accurate readings after the mirror. The power after the polarizer and after the mirror were measured. Once the measurements were complete, the intracavity laser power and polarizer output coupling were derived. The transmissivity of the HR mirror was obtained by using Equation 4.1

$$T_M = \frac{P_T}{P_I} = \frac{P_T \times 0.09}{P_L} \quad (4.1)$$

where  $P_T$  is the transmitted power after the HR mirror,  $P_I$  is the intracavity power,  $P_L$  is the laser power and 0.09 is the transmissivity of the 91% OC. The average transmissivity that was obtained from the HR mirror was 0.00246%.

#### 4.1.2 Polarizer Output Coupling

The output coupling, or the transmission of the polarizer, can be calculated by using Equation 4.2.

$$T_P = \frac{P_L}{P_I} = \frac{P_L \times T_M}{P_T} \quad (4.2)$$

For this equation,  $P_I$  is the intracavity power,  $P_L$  is the average laser power,  $P_T$  is the transmitted power through the HR mirror, and  $T_M$  was the previously calculated mirror transmission. The average transmission for the laser at 100 kHz obtained for the polarizer was around 7.78%.  $P_T$  changed for different repetition-rates. At 100 kHz, a transmission of 13% was obtained after the HV of the PC was tweaked to obtain smaller pulses.

## 4.2 Pulsed Operation

Pulsed operation was achieved by placing the PC and QWP within the laser cavity. For the pulsed operation, the 91% OC was replaced by an HR mirror. The polarizer at Brewster angle acts as the OC in this configuration. This allows the transmission of the horizontally polarized light and transmission of orthogonally polarized light. This allows the laser to be cavity dumped.

### 4.2.1 Energy Output

The TruMicro 7050 is capable of producing pulses with up to 80mJ of energy. Since the laser is pulsed by means of cavity dumping, most of the energy remains inside the laser cavity. For the TruMicro, this intracavity energy is enclosed in a pulse of 100 ns. The intracavity energy is almost ten times greater than that dumped.

The laser was operated at 5 kHz, 10 kHz, and 100 kHz. The maximum safe pump powers for these frequencies were 55%, 85% and around 70% of the total available diode power, respectively. Running the laser past these values will cause chaotic behavior and possible damage to the optics. A plot of the pulse energy versus pump power can be seen in Figure 4.2. Similar to the power growth, the energy grows linearly with respect to the pump power. The 10 kHz operation had the best combination of energy and power output for the system.

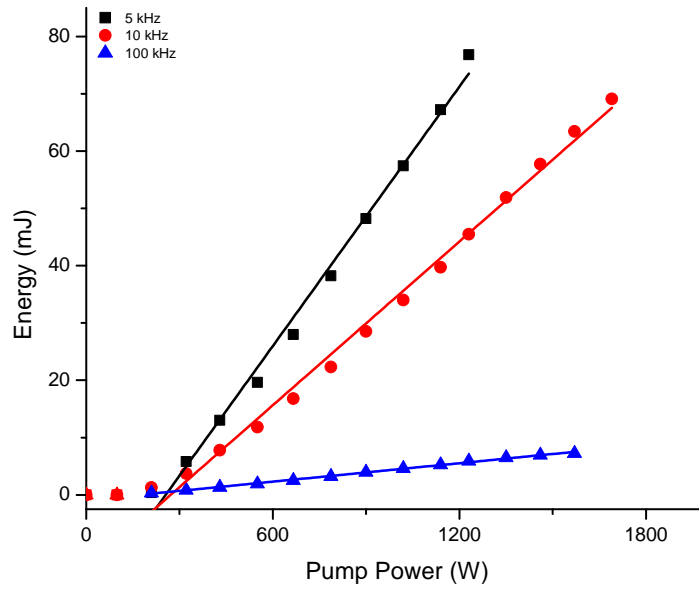


Figure 4.2: Trupf TruMicro 7050 Energy Output

#### 4.2.2 Average Power

The laser system produces average powers up to 400 W at 5 kHz and 800 W at 10 and 100 kHz. These correspond to the energy limits for the corresponding frequencies. Figure 4.3 shows the slope efficiency and optical to optical efficiencies for the system during pulsing. The slope efficiencies for the system were 37.7%, 47.6,% and 53.7% for the 5, 10 and 100 kHz, respectively. The optical to optical efficiencies tend to increase with pump power at 5 kHz and 10 kHz, where they approach 31% and 41%. At 100 kHz, the optical efficiency reached a maximum of 48% before decreasing. These values are comparably smaller than the measured values for CW, at which the slope efficiencies were above 60% and the optical-to-optical efficiencies approached 55%.

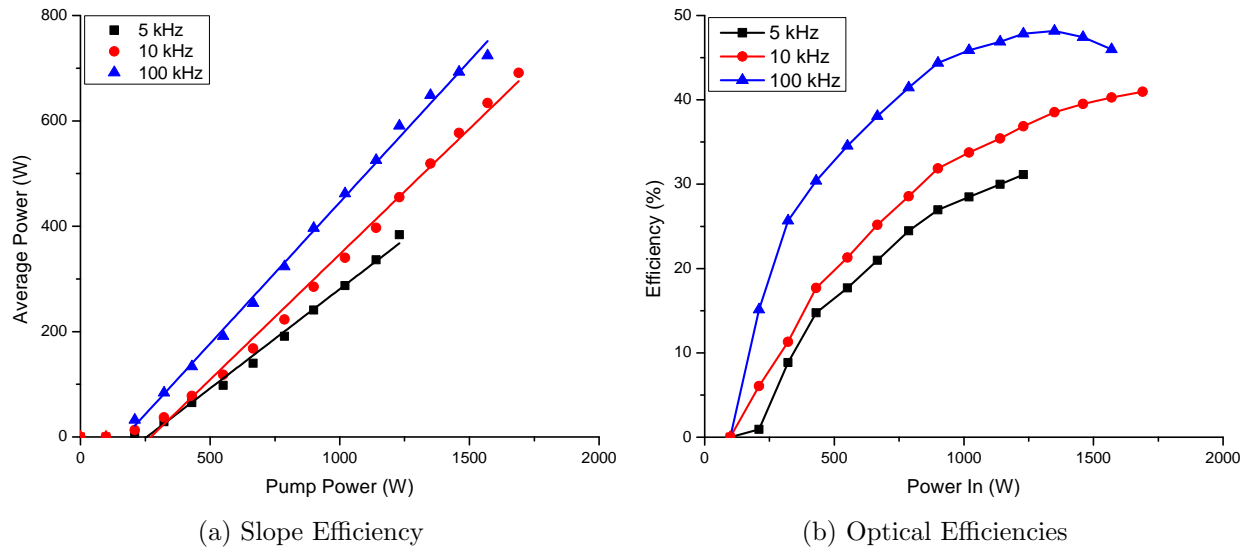


Figure 4.3: Trumpf TruMicro 7050 Pulsed Efficiencies

### 4.2.3 Pulse Duration

Small changes to the pulse duration were observed as a function of pumping power and gain in the system. Figure 4.5 shows the pulse durations versus the pump power. The pulse duration ranged from 30 to 42 ns. As the pump power increased for higher repetition rates, the pulse duration started to stabilize for the higher repetition rates. At 5 kHz, the pulse duration was somewhat inconstant.

The TruMicro is capable of producing laser pulses with different pulse durations. To control the pulse duration of the laser, the high voltage that drives the Pockels cell can be adjusted. By increasing the HV supply for the Pockels cell, the pulse duration of the laser pulse can be shortened. Starting the laser near the maximum high voltage caused a fault, so it was started with the high voltage set at the 60% base level and then increased. The

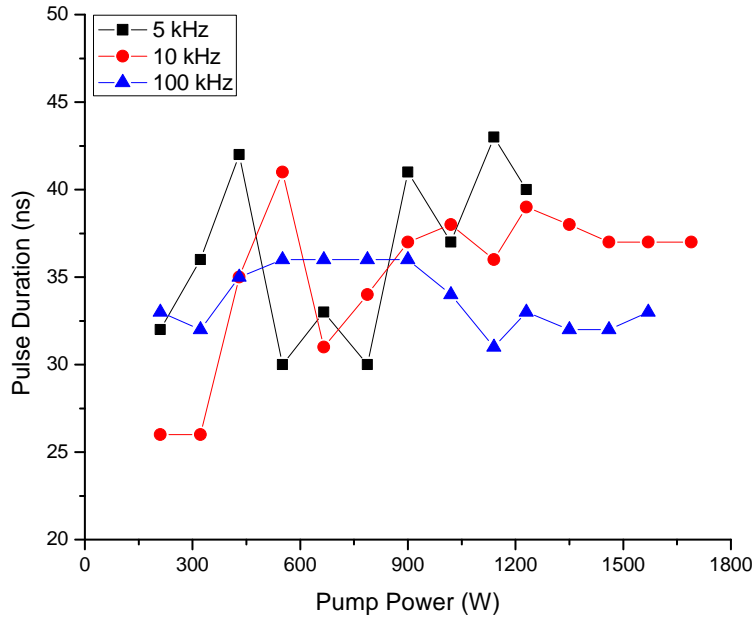


Figure 4.4: Trumpf TruMicro 7050 Pulse Duration at Various Frequencies

laser was interfaced by means of using a computer terminal to send the voltages to the laser processor. If the voltage is too low, there is possibility of chaotic oscillations between pulses. When voltage was changed, the waveplate orientation was adjusted to optimize the pulse.

The shortest pulse duration was observed as 17.7 ns, while operating the laser at 10 kHz, 30% of input power, and providing 100% HV to the PC. An example of the narrow pulses can be seen in Figure 4.5. This pulse, generated by operating the laser at a similar configuration to that aforementioned, had a duration of 18.1 ns.

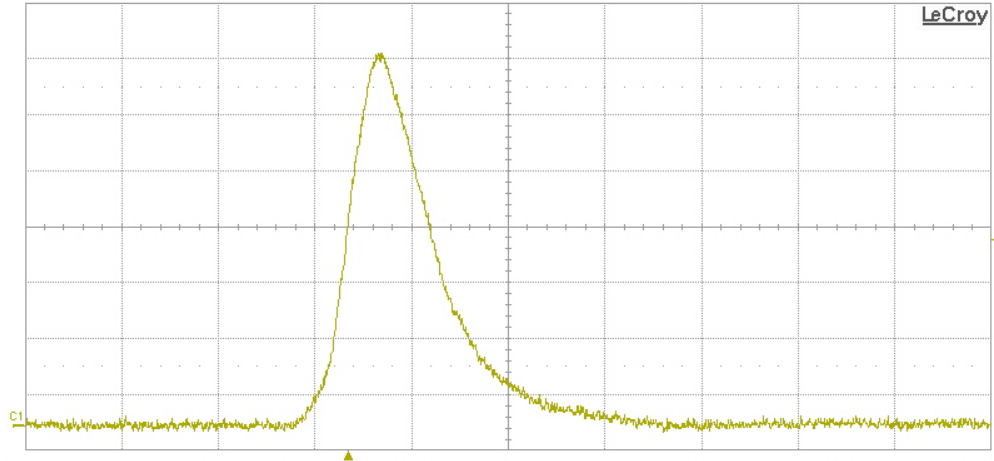


Figure 4.5: Trumpf TruMicro 7050 Pulse

#### 4.2.4 Peak Power

Peak power is the measure of the radiated power that is produced by each laser pulse. This is a relation of energy and pulse duration. The peak power of a pulsed laser can be several orders of magnitude higher than the power of a CW laser [20]. Figure 4.6 shows the trend of peak power with respect to pump power. For repetition rates of 5 and 10 kHz, pulses with peak powers close to 2 MW were observed.

### 4.3 Beam Quality

Thin disk lasers can yield high powers while maintaining good beam qualities. Near diffraction-limited thin disk lasers with powers greater than 100 W have been reported [44]. The  $M^2$  value is one of several ways to describe the beam quality of a laser. The smaller the  $M^2$  value, the smaller the beam divergence is. Beam divergence is a quantization of



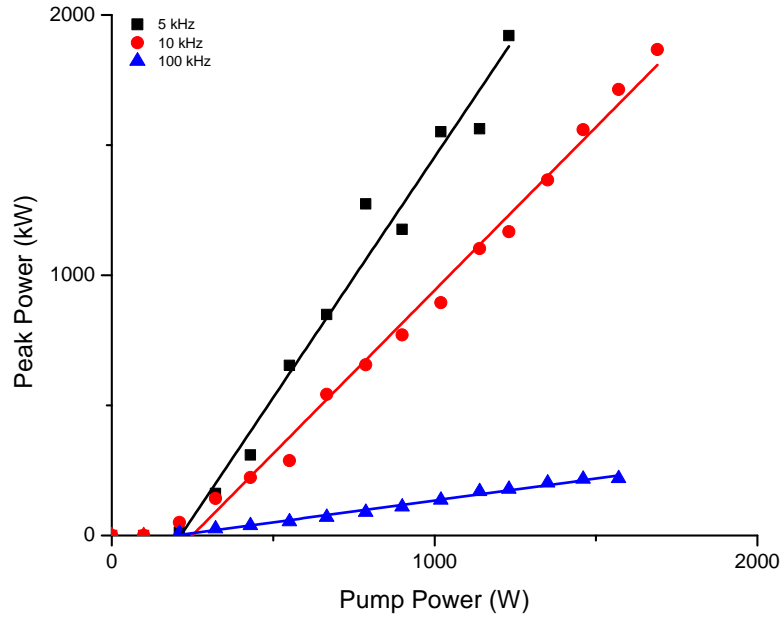


Figure 4.6: Trumpf TruMicro 7050 Peak Powers

the increase of a laser beam's size as compared to its waist. The  $M^2$  factor is defined in Equation 4.3, where  $\Theta$  is the half angle of the beam's divergence,  $W_0$  is the beam radius at waist (for a multimode beam), and  $\lambda$  is the laser wavelength [18]:

$$M^2 = \Theta \frac{W_0 \pi}{\lambda} \quad (4.3)$$

Achieving diffraction-limited beam quality is usually unattainable for most high power solid-state lasers, which rely on a larger gain medium that is more prone to thermal lensing. Typically, as the power of the pump and the laser go up, the beam quality of the laser goes down. Even though thin disk lasers in the kilowatt range have moderate  $M^2$  values, their

beams generally have less divergence than other types of solid-state lasers operating in the same power range.

Another method to quantify the beam quality is by using the beam parameter product. This product demonstrates the amount of spatial divergence per the divergence angle. It can be obtained by using Equation 4.4.

$$BPP = \Theta W_0 = M^2 \frac{\lambda}{\pi} \quad (4.4)$$

#### 4.3.1 Measurement Technique

The measurement technique used to determine the beam quality can be seen in Figure 4.7. A high energy dielectric attenuator (CVI Melles Griot, HPDA-1064-3.00-20) was used to reflect 90% onto a chilled beam dump, the rest was transmitted through the attenuator. 4% of the transmitted light is reflected off the fused silica (quartz) wedge and the rest is dumped. Neutral density (ND) filters dampen the beam before reaching the focusing lens. The focusing lens was a plano-convex BK7 lens with a diameter of 50.8 mm and 100 mm focal length. A 10x microscope objective was used to image the focused beam onto a Spiricon beam profiler. The beam profiler used for this experiment was the LBA-FW-SCOR20. It has a spectral response from 350-1320 nm, 1600 x 1200 pixels and can resolve a maximum beam size of 7 mm x 5.3 mm [52]. Some beam profiles at 20% and 50% are shown in Figure 4.8 and in Figure 4.9.

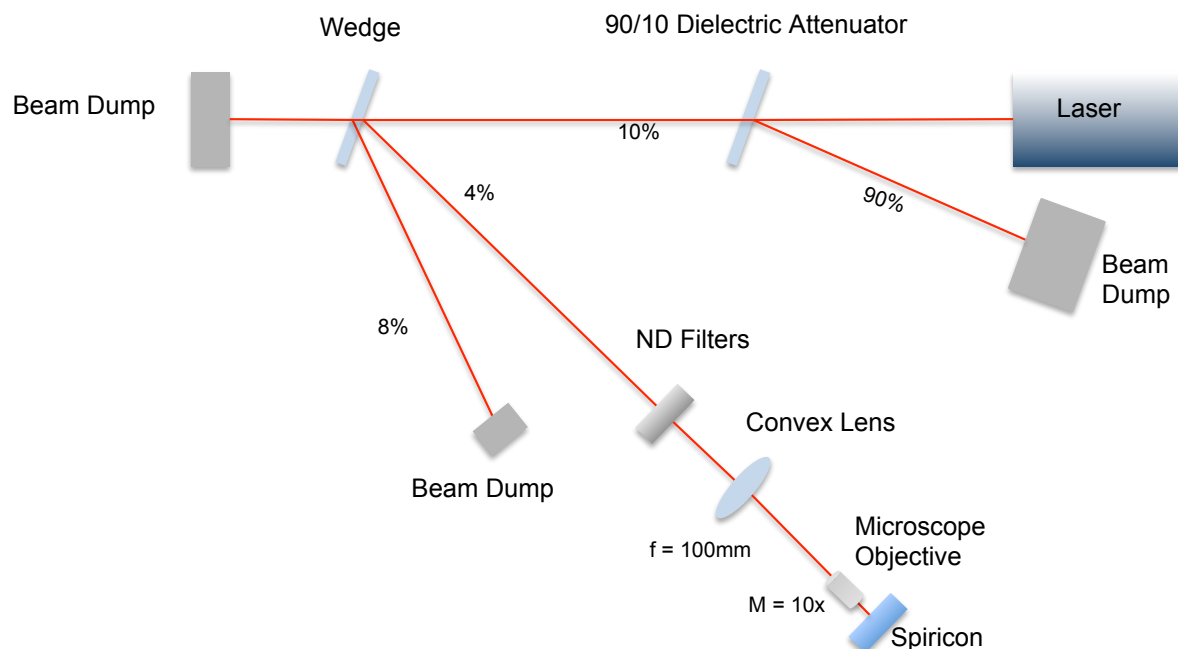


Figure 4.7: Trumpf TruMicro 7050 Beam Measurement Technique

The second moment ( $D4\sigma$ ) beam size was obtained by using the Spiricon laser beam analysis (LBA) software. The  $D4\sigma$  beam size is the ISO standard for measuring beam spot sizes for multimode beams. It describes the beam size as four standard deviations of the beam intensity distribution. The  $D4\sigma$  for a Gaussian beam ( $M^2=1$ ) is the equivalent of the  $1/e^2$  measurement [53, 54, 55]. The total magnification of the system was calculated by using a resolution chart to determine an accurate beam size. The lens was shifted to observe the waist at focus. The data from the waist was used with Equation 4.5 and Equation 4.6 to determine the Rayleigh range ( $z_R$ ) and  $M^2$  [56].

$$2W(z) = 2W_0 \left[ 1 + (z - z_0)^2 / z_R^2 \right]^{1/2} \quad (4.5)$$

$$z_R = \frac{\pi W_0^2}{\lambda M^2} \quad (4.6)$$

The TruMicro 7050's was determined to be, on average, 10.97 times diffraction-limited. The  $M^2$  value incremented with pump power due to an increased number of modes that lased reaching a maximum value of 14 times diffraction-limited.. The BPP was calculated using Equation 4.4 to be 3.60 mm\*mrad on average and 4.59 mm\*mrad as the maximum. By using Equation 4.3, the divergence angle,  $\Theta$ , was calculated to be 71.19 mrad.

Figure 4.8 and Figure 4.9 show the far field beam profiles of the Trumpf laser system at different operations (CW and pulsed). Multimode operation is observed throughout all of the different operations. The beams had an average radius of 50  $\mu\text{m}$ . The differences between the different repetition-rates and powers were minimal.

#### 4.4 Spectral Characterization

The TruMicro 7050 emission spectrum was observed for CW and pulsed operation. This was done due to Yb:YAG's large bandwidth and the lack of a spectral fixation on the system could produce spectral drift. The Ocean Optics HR4000CG, a ultraviolet to near-infrared (UV-NIR) spectrometer with a 0.75 nm FWHM resolution was used for these measurements. The average center wavelength was 1030.6 nm. The center wavelength drift was  $\pm 350$  pm with a minimum of 1030.3 nm and 1031 nm as the maximum. The linewidth generally increased with pump power from a minimum of 0.7 nm to a maximum of 2.69 nm, with an average of 1.78 nm.

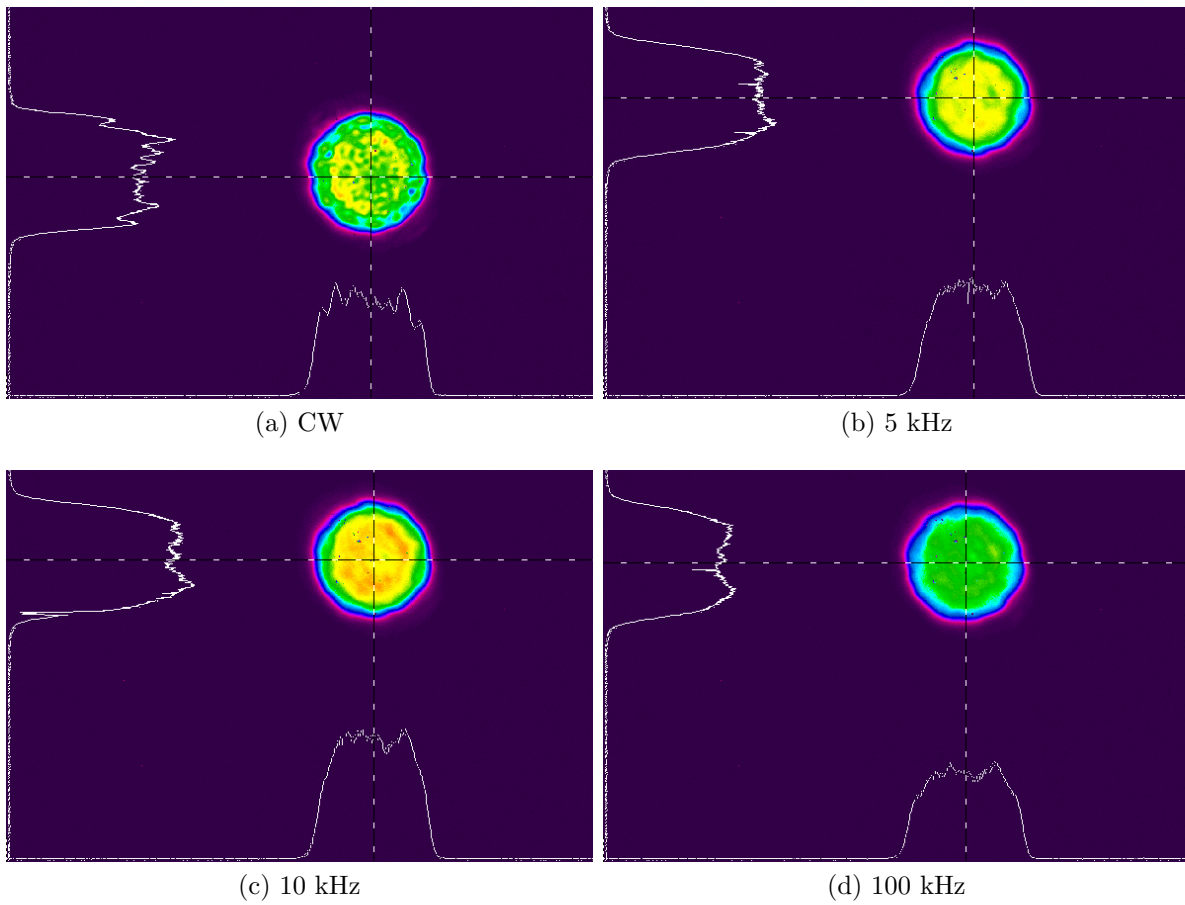


Figure 4.8: Trumpf TruMicro 7050 Far-Field Beam Profiles at 20% Pump Power

## 4.5 Laser Intensity

### 4.5.1 Brightness

The measure of optical power per given area can be described in two ways: the brightness and the radiance of the laser. Focusing the laser beam does not change the brightness of

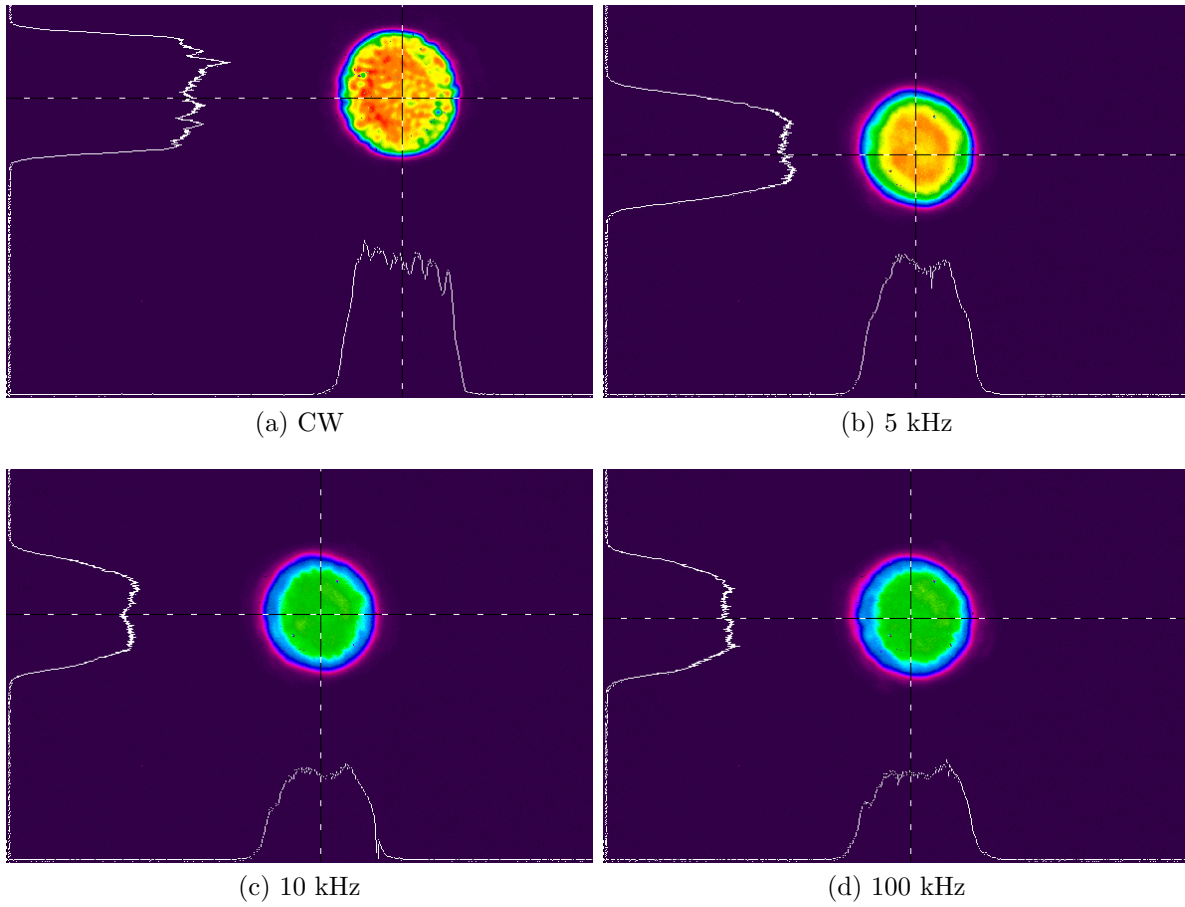


Figure 4.9: Trumpf TruMicro 7050 Far-Field Beam Profiles at 50% Pump Power

such laser [18]. It is a quantity which can be calculated using the equation

$$B = \frac{P}{A\Omega} = \left( \frac{P}{\lambda^2} \right) \quad (4.7)$$

, where  $A = (\pi W_0^2)$ ,  $\Omega = (\pi\Theta^2)$ , and  $\Theta = M^2\lambda/\pi W_0$  [18]. This yields a value of  $6.9 \times 10^8$  W/cm<sup>2</sup>sr as the maximum brightness for CW operation, when the power reaches 880 W.

## 4.5.2 Intensity

The intensity of the laser, also called radiance, quantifies the power over a given area. This unit can be changed by focusing the laser beam by means of a converging lens. The laser intensity can be calculated using the equation

$$I = \frac{P_{peak}}{A} = \frac{E}{A\tau} \quad (4.8)$$

, where  $P_{peak}$  is the peak power,  $E$  is the pulse energy,  $A$  is the beam area and  $\tau$  is the pulse duration. Using this equation, a maximum intensity of  $2.56 \times 10^{10}$  W/cm<sup>2</sup> was calculated (at 5 kHz, 55% of input power;  $E = 76.8$  mJ,  $\tau = 40$  ns).

This measure is very crucial to the development of EUV. For efficient EUV generation, a radiance of at least  $1.5-2 \times 10^{11}$  W/cm<sup>2</sup> is required. Having a value too low will not produce the desired plasma temperature and a value too high will increase the level of debris in the system. Using a telescope to expand the beam so as to cover the entire lens will yield a smaller divergence and hence a smaller beam waist. This process will yield a higher intensity ( $\sim 6 \times 10^{11}$  W/cm<sup>2</sup>) when the beam is increased from  $\sim 10$  mm to 50 mm. Achieving such a high intensity from such setup gives the possibility of using a longer focal length lens (larger beam size at focus) to achieve the necessary intensity for EUV. Using the focusing element at a longer distance diminishes the debris at the lens and promotes a longer lifetime.

## 4.6 Improvements

In order to improve the beam quality without reducing the output power, several changes can be made to the laser cavity. These include extending the length of the folding arm and changing some of the planar HR mirrors with some curved HR mirrors. Initial calculations performed by Trumpf and CREOL scientists modeled that using curved mirrors with radii of 2-5 meters would yield a better beam quality.

### 4.6.1 Damage Thresholds

If some of the cavity parameters are changed, it is important to remember the damage threshold of the intracavity optics, since these experience a greater fluence than those outside the cavity. The damage threshold for the disk itself is approximately  $5 \text{ J/cm}^2$ , for the PC and QWP it is  $10 \text{ J/cm}^2$  and for the mirrors it is  $30 \text{ J/cm}^2$ . Since the intracavity folding mirror is exposed to light traveling in both directions in the cavity, its threshold is half of the mentioned value.



## CHAPTER 5 LASER MODELING

### 5.1 LASCAD

The laser models performed for this thesis were done with LASCAD. This software allows the user to design a laser cavity and provides information such as resonator stability, output power, energy, pulse duration, beam profile, and thermal effects. LASCAD provides the user with four tools: Finite Element Analysis, Laser Power CW, Beam Propagation, and Dynamic Multimode Analysis. Each of these components will be discussed in further detail. A current limitation in the software is that the Beam Propagation and the Dynamic Multimode Analysis only work for 4-level systems, such as Nd:YAG. Since Yb:YAG is a Quasi-3 level system, these algorithms will not create valid results.

The laser resonator can be designed on the main screen, which has a section to incorporate the optics and observe the fundamental mode propagation. Each of the optical components' properties can be specified. Some of these properties include radius of curvature, size, angle of incidence, index of refraction, aperture size, and location. It is able to generate the beam size for the fundamental mode throughout the cavity. LASCAD uses the laser ABCD matrices to compute the beam propagation throughout the laser cavity [57]. Based on these

calculations, it is able to determine the stability criterion and provide information to the user, including a stability curve. LASCAD is able to adapt the stability curve to changes in the cavity design in real time. More information regarding laser resonator stability can be found in Section 2.1.2.

### 5.1.1 Finite Element Analysis

The Finite Element Analysis, FEA, computes the heat and stress induced characteristics of the laser system. This code can be run after the designed laser resonator is within the stability limits. The FEA has several input types, such as the laser gain material, the pumping scheme and the cooling mechanism. The software allows for the selection of gain media type, size, geometry and crystal configuration. LASCAD provides data files for several materials, such as Nd:YAG, Nd:YVO<sub>4</sub>, Nd:YLF, Yb:YAG and Yb:KGW. The different properties of each can be changed within the FEA GUI (doping concentration, index of refraction, thermal conductivity, etc.). The FEA is also able to generate results for a laser gain crystal with doped and undoped regions [58]. For the pumping scenario, the pump spot size, location, divergence, symmetry and power can be declared. The cooling method and reference temperature for the laser can also be established. FEA allows for fluid or contact cooling.

The code discretizes the crystal into a 3 dimensional grid and iterates through these a defined amount of times. Running the FEA generates the data used for simulating thermal

lensing within the laser cavity. It also produces three dimensional representations of the crystal heat load, temperature and stress. The FEA relies on equations which describe heat conduction, structural deformation and absorption [59]. The rest of the algorithms within LASCAD depend on the results from the FEA to generate results.

### 5.1.2 Laser Power CW

The Laser Power algorithm provides an accurate representation of what the laser output power for a given cavity configuration. This code depends on the pump wavelength, pump power, the output mirror reflectivity (output coupling), mode operation, and the results from the FEA code. The user has the capability of changing these values, as well as to choose or ignore intracavity apertures, to obtain the desired laser modes and power. This code generates the output power with respect to the input power with a constant output coupling or the output power with respect to the input output coupling with a constant input power.

The Laser Power algorithm uses Laser Rate Equations to provide the power data. These equations can be simplified into the relation which describes output power for various inputs.

The power can be obtained using the equation

$$P_{out} = h\nu_L S_L \frac{c(-\ln(R_{out}))}{2L} \quad (5.1)$$

, in which  $h$  is Planck's constant,  $c$  is the speed of light in vacuum,  $\nu_L$  is the laser light frequency,  $R_{out}$  is the OC reflectivity,  $L$  is the optical path length, and  $S_L = \tau_c \eta_p S_p$  is the total number of lasing photons [60]. By further expanding this equation and adding a crystal volume dependence, a more accurate result is obtained. When considering a Quasi-3 level system, the equation expands into

$$P_{out} = \frac{hcT_M}{\lambda_L T_T} \int \int \int_a \frac{q_\sigma \eta_p \lambda_p P_p p_0 / (hc) - (q_\sigma - 1) N_t / \tau}{q_\sigma + \frac{hcT_M}{P_{out}(S_{GR} + S_{GL})\sigma\tau\lambda_L}} dV \quad (5.2)$$

, in which  $\lambda_l$  is the laser wavelength,  $P_p$  is the pump power,  $\lambda_p$  is the pump wavelength,  $\eta_p$  is the pump efficiency,  $\tau$  is the spontaneous lifetime,  $T$ 's are the cavity losses, and  $q_\sigma = 1 + \frac{\sigma_a}{\sigma_e}$ , where  $\sigma_a$  and  $\sigma_e$  are the absorption and emission cross section, respectively [60].

### 5.1.3 Beam Propagation

The Beam Propagation Method, BPM, algorithm develops three dimensional intensity and phase intensity profiles for the beam as it propagates through the laser cavity. The code is able to take into account the interference and diffraction effects from intracavity apertures and the thermal lens within the crystal. BPM uses a FFT Split-Step Beam Propagation Method to perform these computations [61]. The beam shape, which can be seen in a three dimensional contour map, will fluctuate as it encounters the different optics or suffers from diffraction effects within the cavity throughout several iterations. It is also capable of

demonstrating multimode laser operation. It provides the user with the flexibility of selecting any point in the map to determine the intensity value.

#### **5.1.4 Dynamic Multimode Analysis**

The Dynamic Multimode Analysis, DMA, is the last piece of code that is part of LASCAD to completely model and characterize a possible laser system. This code deals with multimode operation and the time domain characteristics of the laser. It is able to generate laser pulses and provide information such as pulse duration and energy for such pulses. It also generates time dependent  $M^2$  values and upper energy level population for the laser medium. The DMA provides the user with many variables which can be tweaked to meet the laser requirements. This code uses the data from the FEA and from the eigenmodes from the ABCD matrices to perform its analysis by means of time dependent multimode laser rate equations [62].

## **5.2 Design**

### **5.2.1 Cavity Layout**

The Trumpf TruMicro laser cavity was modeled using LASCAD. Since the model was operated in the CW regime, some changes were done to simplify the cavity. A flat mirror was placed instead of the polarizer and a curved mirror was placed behind the thin disk, to

account for the curvature of the disk and the HR coatings at the end surface of the disk. The OC had a reflectivity of 91%. The layout of this simplified cavity can be seen in Figure 5.1.

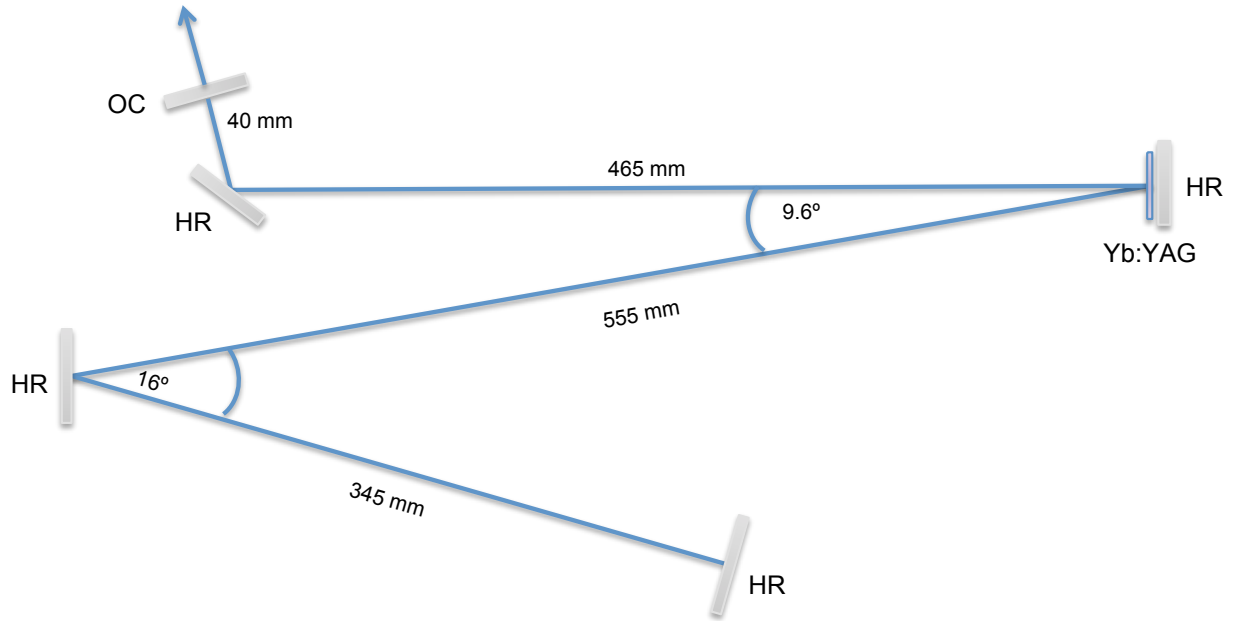


Figure 5.1: LASCAD Cavity Configuration

### 5.2.2 Pumping Technique

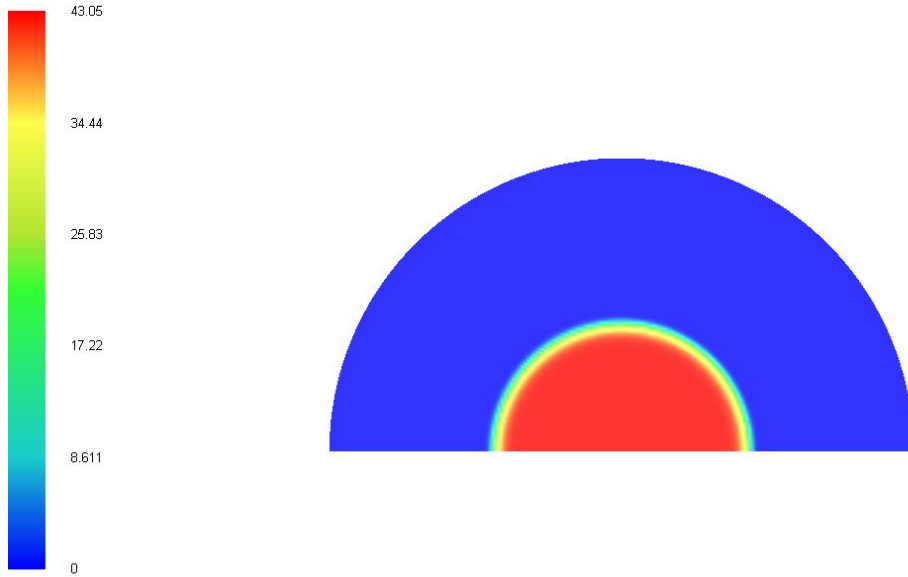
The Finite Element Analysis involves many laser gain and pumping parameters, ranging from size and geometry to different coefficients. In order to properly use the FEA, the pumping and disk geometry were introduced, as provided from Trumpf, with several assumptions. The pumping power was set to the maximum of 2250 W, with a spot radius of  $3150 \mu\text{m}$  and a top hat beam profile. A disk thickness of  $200 \mu\text{m}$  was used, with a diameter of 14mm. Since Yb:YAG is a Quasi-3 level system, it was set as a 3 level material in the FEA. The

heat sink was cooled to a temperature of 343.15 K. The absorption of the Yb:YAG, which would be affected by a different doping concentration, was not changed for the simulation. The thermal conductivity was 0.014 W/mmK, the thermal expansion coefficient was  $7 \times 10^{-6} \text{ K}^{-1}$ , the index of refraction was 1.82 and the doping concentration was  $\sim 5\%$ .

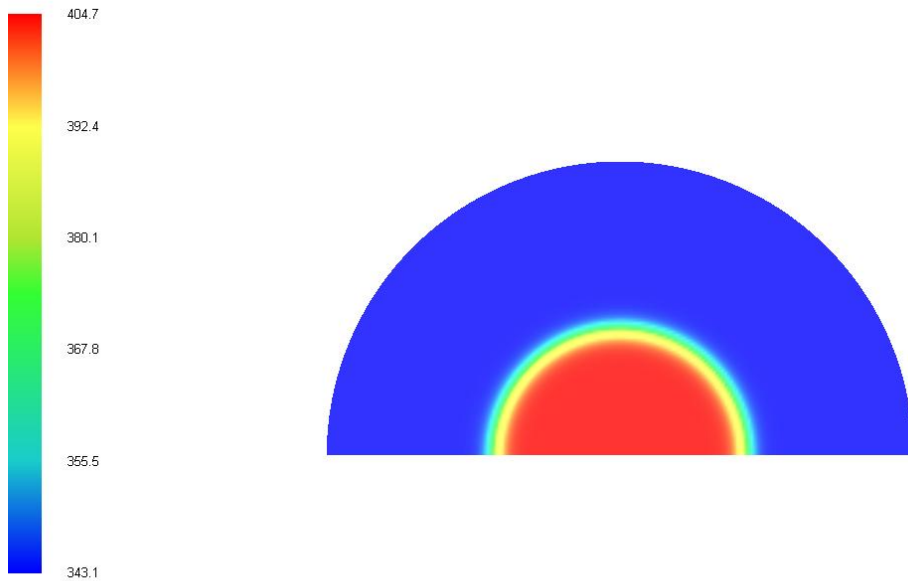
## 5.3 Results

### 5.3.1 Finite Element Analysis

LASCAD is able to efficiently model the thermal effects that the laser gain media encounters during pumping. Figure 5.2 and Figure 5.3 represent the results of the thermal and structural computations performed by the FEA code. As it can be noted, outside the central area where the pump spot directly affects the disk, the heat load, temperature and stress are minimal due to the efficient temperature handling of the disk and heat sink. The disk temperature variation ranges from 343.1 K in the outer area to 404.7 K within the pump area. The exterior area has a higher heat load of  $0 \text{ W/mm}^2$  while the interior has a heat load of  $43.05 \text{ W/mm}^2$ . The lowest stress intensity occurred at the edges, with a value of  $8.704 \text{ N/mm}^2$ , and the highest occurred at the center, with  $98.96 \text{ N/mm}^2$ . The von Mises equivalent stress demonstrated a similar pattern with the limits being  $8.3 \text{ N/mm}^2$  at the edges and  $98.32 \text{ N/mm}^2$  at the center of the disk.



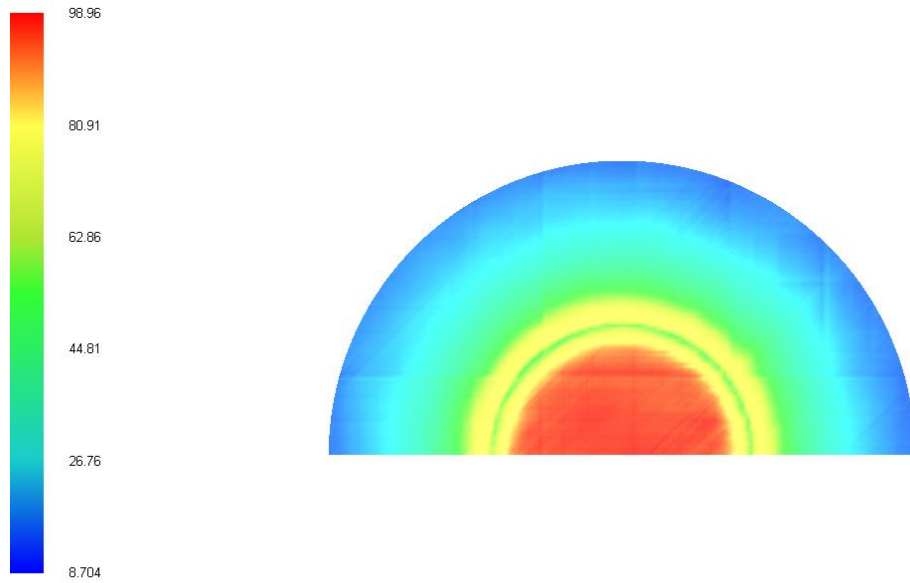
(a) Heat Load



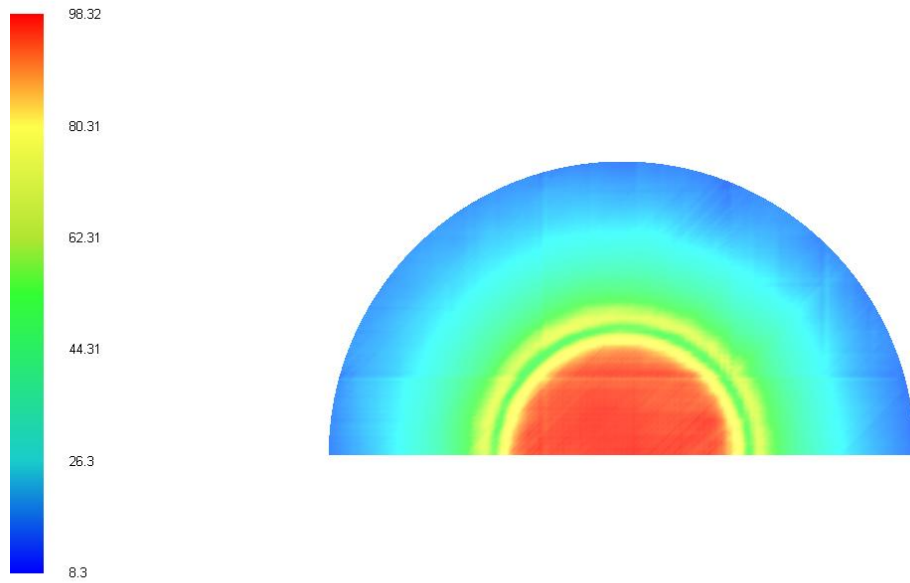
(b) Temperature

Figure 5.2: Thin Disk Thermal Visualizations





(a) Stress Intensity



(b) Von Mises Stress

Figure 5.3: Thin Disk Structural Effects Visualizations

### 5.3.2 Laser Power CW

The results for the Laser Power for the Trumpf Laser proved to be accurate. The slope efficiency for the measured Trumpf laser power values was 66.1%, while the slope efficiency for the LASCAD simulated multimode laser power values was 73.6%. The optical efficiencies for the measured values approached 58%, while the LASCAD simulation approached 62%. The following plots represent the measured and simulated outputs for the laser power and for the optical to optical efficiency.

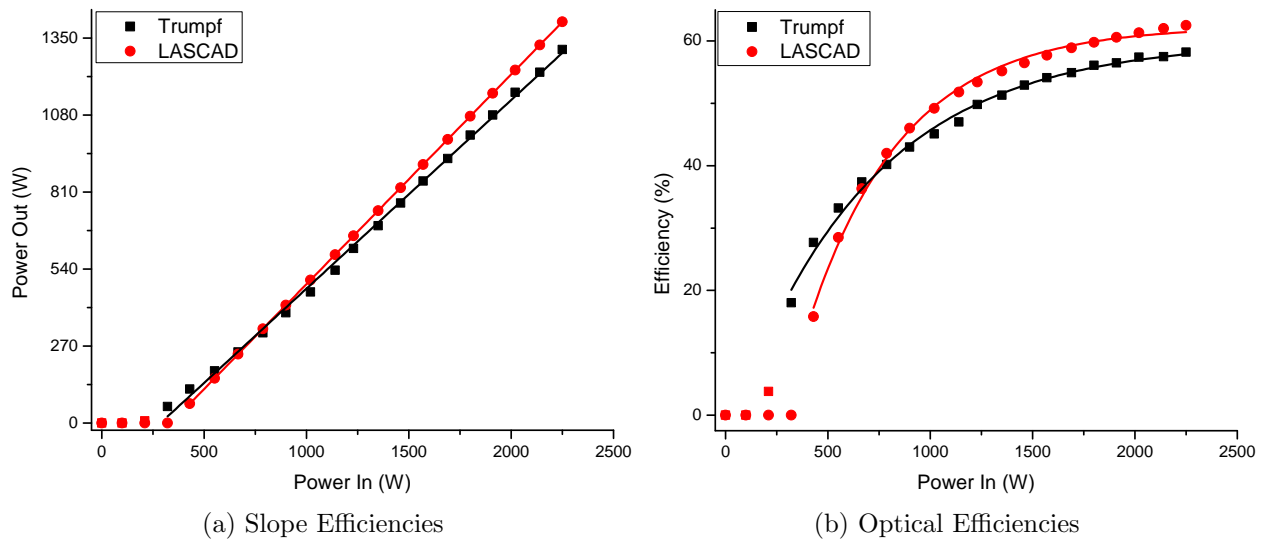


Figure 5.4: Measured vs Simulated Efficiencies

## CHAPTER 6

### CONCLUSION

Thin disk lasers have been established as a predominant laser technology offering low divergence at high power. These lasers have efficient cooling mechanisms which diminishes most of the thermally induced problems associated with the degradation of the beam quality. This makes them more versatile than other solid state lasers, especially at higher powers. 100-200  $\mu\text{m}$  thin disk crystals are soldered directly onto a heat sink and act as mirrors for both the pump and laser radiation. Yb:YAG remains as the predominant gain medium for thin disk lasers due to YAG's capability to be doped with a high concentration of Yb ions. This high doping concentration is necessary to achieve substantial gain in the thin gain medium. Yb:YAG's small QD means that there is less heat produced from non-radiative decay.

The initial characterization of the recently acquired thin disk laser was performed at Schramberg and the final characterization at CREOL. The pulse duration was observed with a fast photodiode and an oscilloscope. A beam profiler was used for the far-field characterization of the laser to determine the beam quality and intensity. The spectral emission of the laser was characterized using a near-IR spectrometer to determine stability.

Simulations from LASCAD provided an in depth perspective of the thermal and stress effects induced in the gain media of the laser cavity during pumping and lasing. Thin disk modeling demonstrated the thermal and stress effects induced on the gain media by pumping and lasing mechanisms. A top hat thermal gradient was observed, which leads to a decreased thermal lensing. This simulation will be useful to observe laser cavity optimization for this laser system.

### 6.1 Future Work

In the near future, this laser will be used to perform high power EUV source development experiments at high repetition rates of up to 100 kHz. The laser and the LPL EUV droplet system will be synchronized at a high repetition rate to conduct these tests. Another aspect to be explored will be the effect of the laser pulse duration on laser plasma stability and conversion efficiency. Previous tests demonstrate conversion efficiencies of over 2% with pulse durations of 20-30 ns. The TruMicro 7050's pulse duration adaptability will be used to explore the conversion efficiencies for various pulse durations and energies to determine an optimum operation.

The models that were performed using LASCAD will be used to determine if the beam quality and power can be enhanced by laser cavity modifications. The simulations will be updated when LASCAD provides support to Quasi-3 level systems and cavity dumping. The new version should provide more insight of the temporal characteristics of the laser and how they will be affected by changing the laser resonator.

**APPENDIX A**  
**COPYRIGHT PERMISSION LETTER**

**ELSEVIER LICENSE  
TERMS AND CONDITIONS**

May 03, 2010

---

This is a License Agreement between Omar R Rodriguez ("You") and Elsevier ("Elsevier") provided by Copyright Clearance Center ("CCC"). The license consists of your order details, the terms and conditions provided by Elsevier, and the payment terms and conditions.

**All payments must be made in full to CCC. For payment instructions, please see information listed at the bottom of this form.**

Supplier	Elsevier Limited The Boulevard, Langford Lane Kidlington, Oxford, OX5 1GB, UK
Registered Company Number	1982084
Customer name	Omar R Rodriguez
Customer address	4000 Central Florida Blvd. Orlando, FL 32816
License Number	2421430790629
License date	May 03, 2010
Licensed content publisher	Elsevier
Licensed content publication	Journal of Luminescence
Licensed content title	Rare-earth-doped sesquioxides
Licensed content author	K Petermann, G Huber, L Fornasiero, S Kuch, E Mix, V Peters, S.A Basun
Licensed content date	May 2000
Volume number	87-89
Issue number	
Pages	3
Type of Use	Thesis / Dissertation
Portion	Figures/tables/illustrations
Number of Figures/tables/illustrations	2
Format	Both print and electronic
You are an author of the Elsevier article	No
Are you translating?	No
Order Reference Number	
Expected publication date	Dec 2010
Elsevier VAT number	GB 494 6272 12
Permissions price	0.00 USD
Value added tax 0.0%	0.00 USD
Total	0.00 USD

## LIST OF REFERENCES

- [1] J. Gordon, H. Zeiger, and C. Townes, "The Maser - New Type of Microwave Amplifier, Frequency Standard and Spectrometer," *Physical Review*, vol. 99, no. 4, pp. 1264–1274, 1955.
- [2] A. Schawlow and C. Townes, "Infrared and optical masers," *Physical Review*, vol. 112, no. 6, pp. 1940–1949, 1958.
- [3] T. Maiman, "Stimulated optical radiation in ruby," *Nature*, vol. 187, pp. 493–494, 1960.
- [4] J. C. Ion, *Laser Processing of Engineering Materials*. Elsevier, 2005.
- [5] J. D. Majumdar and I. Manna, "Laser processing of materials," *Sadhana*, vol. 28, pp. 495–562, 2003.
- [6] H. K. Soong and J. B. Malta, "Femtosecond Lasers in Ophthalmology," *American Journal of Ophthalmology*, vol. 147, no. 2, pp. 189–197, 2009.
- [7] J. Sulewski, "Historical survey of laser dentistry," *Dental Clinics of North America*, vol. 44, pp. 717–752, 2000.
- [8] L. Goldman, "Future of Laser Dermatology," *Lasers in Surgery and Medicine*, vol. 22, pp. 3–8, 1998.
- [9] "Industry Fact Sheet," Semiconductor Industry Association, 2010.
- [10] B. G. Eynon, "Extreme Ultraviolet Lithography," pp. 1–30, 2009.
- [11] "Lithography," International Technology Roadmap for Semiconductors, 2009.
- [12] C.-S. Koay, "Radiation studies of the tin-doped microscopic droplet laser plasma light source specific to EUV lithography," PhD, University of Central Florida, 2006.
- [13] M. Richardson, "Extreme Ultraviolet Lithography," pp. 121–173, 2009.
- [14] K. Takenoshita, S. George, T. Schmid, C.-S. Koay, and et al., "Characterization of the Tin-doped droplet laser plasma EUVL sources for HVM," *SPIE*, vol. 6517, p. 113, 2007.
- [15] T. Schmid, S. George, J. Cunado, S. Teerawattanasook, R. Bernath, and et al., "High repetition-rate LPP-source facility for EUVL," *SPIE*, vol. 6517, p. 107, 2007.

- [16] A. Giesen, H. Hügel, A. Voss, K. Wittig, U. Brauch, and H. Opower, “Scalable Concept for Diode-Pumped High-Power Solid-State Lasers,” *Applied Physics B*, vol. 58, pp. 365–372, 1994.
- [17] W. Koechner, *Solid-State Laser Engineering*, 5th ed. Springer, 1999.
- [18] O. Svelto, *Principles of Lasers*, 4th ed. Plenum Press, 1998.
- [19] F. Träger, *Springer Handbook of Lasers and Optics*. Springer, 2007.
- [20] F. McClung and R. Hellwarth, “Giant Optical Pulsations from Ruby,” *Journal of Applied Physics*, vol. 33, no. 3, pp. 828–829, 1962.
- [21] R. Paschotta, *Encyclopedia of Laser Physics and Technology*, 1st ed. Wiley-VCH Verlag GmbH & Co., 2008.
- [22] C. Stolzenburg, A. Voss, T. Graf, M. Larionov, and A. Giesen, “Advanced pulsed thin disk laser sources,” *Proceedings of SPIE*, vol. 6871, 2008.
- [23] W. Hook, R. Dishington, and R. Hilberg, “Laser Cavity Dumping Using Time Variable Reflection,” *Applied Physics Letters*, vol. 9, no. 3, 1966.
- [24] J. Dong, M. Bass, Y. Mao, P. Deng, and F. Gan, “Dependence of the  $\text{Yb}^{3+}$  emission cross section and lifetime on temperature and concentration in yttrium aluminum garnet,” *Journal Of The Optical Society of America B Optical Physics*, vol. 20, pp. 1975–1979, 2003.
- [25] W. Martin and J. Chernoch, “Multiple internal reflection face-pumped laser,” Patent 3,633,126, January, 1972.
- [26] J. Eggleston, T. Kane, K. Kuhn, J. Unternahrer, and R. Byer, “The Slab Geometry Laser - Part I: Theory,” *IEEE Journal of Quantum Electronics*, vol. QE-20(3), pp. 289–300, 1984.
- [27] E. Snitzer, “Proposed Fiber Cavities for Optical Masers,” *Journal of Applied Optics*, vol. 32, no. 1, pp. 36–39, 1961.
- [28] J. Almasi and W. Martin, “Face-Pumped, Face-Cooled Laser Device,” Patent 3,631,362, December, 1971.
- [29] A. Giesen, H. H, A. Voss, K. Wittig, and et al., “Diode-Pumped High-Power Solid-State Laser: Concept and First Results with  $\text{Yb}:\text{YAG}$ ,” in *OSA Proceedings on Advanced Solid-State Lasers*, vol. 20, 1994, pp. 91–94.
- [30] I. Johannsen, S. Erhard, D. Müller, C. Stewen, A. Giesen, and K. Contag, “ $\text{Nd}:\text{YAG}$  thin disk laser,” *Advanced Solid State Lasers*, vol. 34, pp. 137–143, 2000.



- [31] J. Gao, M. Larionov, J. Speiser, and A. G. et al., “Nd:YVO<sub>4</sub> Thin Disk Laser with 5.8 Watts Output Power at 914nm,” 2002, pp. 175–176.
- [32] N. Berner, A. Dienen, E. Heumann, G. Huber, and et al, “Tm:YAG: A Comparison between endpumped Laser-rods and the 'Thin-Disk'-Setup,” *Advanced Solid State Lasers*, vol. 26, pp. 463–467, 1999.
- [33] M. Larionov, J. Gao, S. Erhard, A. Giesen, and et al, “Thin Disk Laser Operation and Spectroscopic Characterization of Yb-doped Sesquioxides and Potassium Tungstates,” *Advanced Solid State Lasers*, vol. 50, pp. 625–631, 2001.
- [34] M. Fox, *Optical Properties of Solids*. Oxford University Press, 2001.
- [35] H.-Y. Lin, J. Guo, D.-Y. Ning, S.-W. Wang, and H.-M. Tan, “LD end-pumped intracavity frequency doubled Yb:YAG laser,” *Optics Communications*, vol. 281, pp. 6065–6067, 2008.
- [36] W. T. Silfvast, *Fundamentals of Lasers*, 2nd ed. Cambridge University Press, 2004.
- [37] K. Petermann, G. Huber, L. Fornasiero, S. Kuch, and et al., “Rare-earth-doped sesquioxides,” *Journal of Luminescence*, vol. 87-89, pp. 973–975, 2000.
- [38] E. Kanchanavaleerat, D. Cochet-Muchy, M. Kokta, J. Stone-Sundberg, and P. S. et al., “Crystal growth of high doped Nd:YAG,” *Optical Materials*, vol. 26, pp. 337–341, 2004.
- [39] X. Xu, Z. Zhao, P. Song, J. Xu, and P. Deng, “Growth of high-quality single crystal of 50 at.% Yb:YAG and its spectral properties,” *Journal of Alloys and Compunds*, vol. 364, pp. 311–314, 2006.
- [40] M. Larionov, J. Gao, S. Erhard, A. Giesen, and et al., “Thin Disk Laser Operation and Spectroscopic Characterization of Yb-doped Sesquioxides and Potassium Tungstates,” in *OSA TOPS on Advanced Solid-State Lasers*, vol. 50, 2001, pp. 625–631.
- [41] A. Demidovich, A. Kuzmin, G. Ryabstev, M. Danailov, W. Strek, and A. Titov, “Influence of Yb concentration of Yb:KYW laser properties,” *Journal of Alloys and Compunds*, vol. 300-301, pp. 238–241, 2000.
- [42] A. Killi, I. Zawischa, D. Sutter, J. Kleinbauer, and et al., “Current status and development trends of disk laser technology,” *Proceedings of SPIE*, vol. 6871, 2008.
- [43] A. Giesen, U. Brauch, I. Johannsen, M. Karszewski, and et al., “High-Power Near Diffraction-Limited and Single-Frequency Operation of Yb:YAG Thin Disc Laser,” in *OSA TOPS on Advanced Solid-State Lasers*, vol. 1, 1996, pp. 11–13.
- [44] A. Giesen, “Thin Disk Lasers: Power scalability and beam quality,” *Laser Technik Journal*, no. 2, pp. 42–45, 2005.

- [45] S. Erhard, M. Karszewski, C. Stewen, A. Giesen, K. Contag, and A. Voss, "Pumping schemes for multi-kw thin disk lasers," in *OSA TOPS on Advanced Solid-State Lasers*, vol. 34, 2000, pp. 78–84.
- [46] S. Erhard, A. Giesen, M. Karszewski, T. Rupp, and et al., "Novel Pump Design of Yb:YAG Thin Disc Laser for Operation at Room Temperature with Improved Efficiency," in *OSA TOPS on Advanced Solid-State Lasers*, vol. 26, 1999, pp. 38–44.
- [47] H. Schlüter, "Thin-disk-laser power scaling improves welding efficiency," *Laser Focus World*, no. 280055, 2006.
- [48] I. Johannsen, S. Erhard, D. Muller, C. Stewen, A. Giesen, and K. Contag, "Nd:YAG thin disk laser," *Advanced Solid State Lasers*, vol. 34, pp. 137–143, 2000.
- [49] G. Hollemann, P. Heist, A. Giesen, and C. Stolzenburg, "Laser and Method for Generating Pulsed Laser Radiation," Patent 11 706 920.
- [50] *Installation Conditions: TruMicro 7050*, TRUMPF Laser GmbH + Co., Aichhalder Straße 39, D-78713 Schramberg, Germany.
- [51] *Service Training, TruDisk 1000*, TRUMPF Laser GmbH + Co., Aichhalder Straße 39, D-78713 Schramberg, Germany.
- [52] "Beam Profile: Wavelength, Temporal, Profile," Ophir-Spiricon Inc. [Online]. Available: <http://www.ophir-spiricon.com>
- [53] "ISO/11146, test methods for laser beam widths, divergence angles and beam propagation ratios," 2005.
- [54] C. B. Roundy, *Current Technology of Laser Beam Profile Measurements*, Spiricon, Inc., Logan, UT 84341.
- [55] *Operator's Manual: Laser Beam Analyzer*, Spiricon, Inc., Logan, UT 84341, 2005.
- [56] J. Thomas Johnston, "Beam propagation ( $m^2$ ) measurement made as easy as it gets: the four-cuts method," *Journal of Applied Optics*, vol. 37, no. 21, pp. 4840–4850, 1998.
- [57] K. Altmann, *Gaussian Beam Propagation Code*, LAS-CAD GmbH, Brunhildenstrasse 9 D-80639 Munich, Germany.
- [58] —, *LASCAD 3.5 Manual*, LAS-CAD GmbH, Brunhildenstrasse 9 D-80639 Munich, Germany, 2009.
- [59] —, *The FEA Code of LASCAD*, LAS-CAD GmbH, Brunhildenstrasse 9 D-80639 Munich, Germany.

- [60] —, *Computation of Laser Power Output for CW Operation*, LAS-CAD GmbH, Brunhildenstrasse 9 D-80639 Munich, Germany.
- [61] —, *LASCAD - The Laser Engineering Tool*, LAS-CAD GmbH, Brunhildenstrasse 9 D-80639 Munich, Germany.
- [62] —, *Dynamic Analysis of Multimode and Q-Switching Operation (DMA)*, LAS-CAD GmbH, Brunhildenstrasse 9 D-80639 Munich, Germany.